RHEOLOGICAL BEHAVIOR OF HIGH MELT STRENGTH

POLYPROPYLENE-BASED MATERIALS

A Dissertation

by

CHIA-YING TSAI

Submitted to the Graduate and Professional School of
Texas A&M University
in partial fulfillment of the requirements for the degree of

DOCTOR OF PHILOSOPHY

Chair of Committee,	Hung-Jue Sue
Committee Members,	Emily Pentzer
	Pavan Kolluru
	Qingsheng Wang
Head of Department,	Ibrahim Karaman

December 2021

Major Subject: Materials Science and Engineering

ABSTRACT

Two types of high melt strength polypropylenes (PP), including long-chain branching (LCB) PP and gel particle-filled PP, have been discussed. This dissertation aims to establish the structure-rheology-morphology-property relationship based on two sets of model PP systems. The linear viscoelasticity of LCB PPs has been systematically studied. The model PPs with a proportional amount of controlled branching structure were prepared with a coupling agent containing bifunctional reactive groups in a twin-screw extruder. The complex viscosity, elasticity, and storage modulus increase with LCB molar fraction. Moreover, a methodology was developed to determine the LCB molar fraction in PPs using gel permeation chromatography and rheological methods. The methodology has been demonstrated to be applied to a commercial high melt strength PP successfully.

This dissertation also focuses on the effect of gel content on PP's linear and nonlinear rheological properties. The PPs filled with the gel particles exhibit pronounced shear-thinning and enhanced zero-shear viscosity. The strain-hardening degree increases significantly with a low loading of gelled particles. Moreover, our SEM and rheological results indicate that the gel particle prepared via grafting-crosslinking modification exhibits a core-shell structure, consisting of a crosslinked PP core and a shell made of grafting chains and constrained matrix chains. Finally, the third part of this dissertation investigates how LCB influences PP's scratch and tensile performance. Scratch resistance of LCB PP was evaluated using a standardized scratch test, followed by visibility analyses,

scratch profile characterization, and materials properties determination. The better elastic

recovery and tensile strength of LCB PP contribute to the enhanced scratch resistance.

DEDICATION

To my beloved family

also like to thank my friends sincerely in College Station. Spending time with you guys in U Club, Stadium view, Parkwest was the best thing I could never dream of during my stay here. I also want to thank my boyfriend, Ying-Kuan Tsai, for your love, support, cute smiles, and wild laughing sounds all the time through my Ph.D. journey.

Finally, I would like to sincerely thank my parents and sisters for their endless support and encouragement. You all are my strength and the reason that I can make it through all the hard times.

CONTRIBUTORS AND FUNDING SOURCES

Contributors

This work was supervised by a dissertation committee consisting of Professor Hung-Jue Sue (advisor, chair of the committee) of the Department of Materials Science and Engineering, Professor Emily Pentzer (committee member) of Department of Materials Science and Engineering, Professor Pavan Kolluru (committee member) of Department of Materials Science and Engineering, and Professor Qingsheng Wang of the Department of Chemical Engineering.

Its contents were completed through the use of the Materials Characterization Facility and the Microscopy and Imaging Center at Texas A&M University. In Chapter III, gel permeation chromatography measurement was done by Dr. Honglan Lu and Dr. Rongti Li. In Chapter IV, X-ray diffraction was done by Ms. Mingzhen Zhao. All other work conducted for the dissertation was completed by the student independently.

Funding Sources

TABLE OF CONTENTS

LIST OF FIGURES

xii

LIST OF TABLES

CHAPTER I

INTRODUCTION

1.1 Background

Polyolefins, especially polyethylene (PE) and polypropylene (PP), have dominated the material market and have been widely used in various industries, such as commodities, automotive, and aerospace. The broad applications of polyolefins are due to their low cost, light weight, excellent corrosion, and good chemical resistance. Additionally, the easy processibility of polyolefin materials combined with the advantages mentioned earlier makes it a promising candidate to replace traditional metal or ceramic parts to reduce the overall product's weight and energy consumption. However, processability for the polymers is not straightforward because of polymeric versatile chemical compositions and molecular structures, such as molecular weight, molecular weight distribution, chain regularity, and molecular architecture. Tuning these chemistry and structural parameters can significantly alter its flow properties.

Moreover, because of the increasing usages of polymer-based materials, scratch resistance and mechanical properties are gaining more attention. This dissertation work focuses on gaining insights into the influences of molecular architecture on flow and mechanical properties. It is hoped that this research work can offer more extensive knowledge about the interrelationship among molecular structure, processibility, and bulk properties.

1

1.2 Research Scope

1.2.1 High Melt Strength Polypropylene

PP, one of the most widely used thermoplastics, has attracted extensive attention because of its several advantages, including relatively good mechanical properties, light weight, and low cost. However, the linear structure of PP exhibits a low melt strength, limiting its applications in the processes dominated by an extensional flow, such as blow molding, thermoforming, and foaming. Great efforts have been made to improve PP's melt strength. For example, incorporating long-chain branching (LCB), blending filler particles, lightly crosslinking, and increasing PP's molecular weight have been developed for improving molten PP's strength [1-4]. Higher melt strength of PP can prevent products from having inhomogeneous wall thickness or collapsed foaming structure. However, little progress has been made to understand the effect of molecular architecture, including branching and crosslinking, on flow and mechanical properties. This is primarily because the control of molecular architecture in polyolefin materials is challenging, especially on an industrial processing scale. This dissertation work presents a methodology to quantify the amount of controlled branching structure in PP. The rheological characteristics of LCB-containing PP are investigated and discussed in detail. Another aspect of this dissertation focuses on the impact of gelled particles, which is another way to improve melt strength of polymers, on flow properties of PPs

1.2.2 Scratch Performance of Polymer-based Materials

The scratch performance of polymers has caught paramount attention in the past decades due to the exponentially growing applications of polymeric materials in electronics, household, commodity, and automotive. Polymeric materials are known for their poor resistance against the surface damages, such as scratching and wearing. Low resistance to the scratch causes not only aesthetic dissatisfaction but also concerns for deteriorating the product performance. A developed ASTM D7027/ISO 19252 standardized scratch test has paved the way to study the scratch behavior of polymeric materials systematically and comprehensively. The scratch test is carried out using a linearly increasing normal load with a geometry. The onsets of different scratch damage transitions, including groove formation, fish-scale cracking, and plowing, can be identified, allowing for straightforward analysis and a fundamental understanding of the structure-property relationship. This dissertation focuses on discussing how the amount of LCB influences the scratch performance of polymers. The tensile properties and creep-recovery measurements were carried out to fundamentally understand the role of LCB in the scratch behavior of PP.

1.3 Research Objectives and Significance

This dissertation work aims to establish an unambiguous structure-property relationship in high melt strength PP and the mechanisms responsible for the observed changes in rheological, scratch, and mechanical properties. The study focuses on developing a methodology to quantitatively evaluate the impact of introducing a LCB

structure onto PP's main backbone. The developed method provides a straightforward pathway using the conventional analytical instruments, i.e., gel permeation chromatography and rheometer, to fundamentally understand the influence of LCB amount on the flow property. Another aspect of this dissertation is to answer the question commonly encountered in the industry: how the gelled particle, usually a by-product during LCB preparation, influences polymers' flow properties of polymers? Interestingly, this dissertation found that the gelled particle serves as a soft filler, altering the entanglement density in polymers to inhibit the mobilities of neighboring matrix chains. Moreover, since the soft filler in the present study is micron-size, to our best of knowledge, there have not yet been well studied how a soft particle moves in a polymer melt at this scale. The rheological behaviors of gel-containing PP elucidate the underlying mechanisms responsible for the enhancement in PP's flow properties.

1.4 Dissertation Layout

The brief introduction presented in this chapter is to provide an overview to the audience for knowing the motivation of the present study. Chapter II presents a literature review regarding molecular architecture, methodologies to evaluate the LCB polymers, and the rheological characteristics of these materials. Chapter II also provides a review of methods to improve PP's melt strength. Chapter III presents a way to quantify LCB molar fraction in PP using a gel permeation chromatography and a rheometer. The influence of LCB content on the rheological properties of PP is investigated. Chapter IV focuses on the effects of micron-sized gelled particles produced in a post-reactor process on flow

behaviors of PP. The mechanisms causing an increase in flow viscosity, storage modulus, and elasticity are described. The studies in Chapter V provide the groundwork for a fundamental understanding of the structure-property relationship of PP containing LCB. The effect of LCB on crystallinity, surface characteristic, scratch performance, and mechanical properties have been explored. Chapter VI summarizes the research outcome, accomplishments, and considerations for future research activities. Finally, the references cited in this dissertation are documented.

CHAPTER II

LITERATURE REVIEW

2.1 Introduction

Molten polymers are usually non-Newtonian fluids, which means that their apparent viscosity is a function of the shear rate or shear rate history. That is, the ratio of shear stress and the shear rate of molten polymer is not a constant. Flow properties of molten polymers are critical because its close association with the processing control of polymeric materials. Moreover, several methods, including macromolecular architecture design (i.e., branching and crosslinking) and nanoparticle incorporation, are implemented to achieve the desired flow properties of polymers. Although the importance of polymer melt's flow property is continuously increasing, the fundamental understanding of the flow behavior of the molten polymers is still being sought after. Additionally, mechanical properties and scratch performance are crucial for establishing the structure-property relationship and realizing these polymeric materials for practical applications. Therefore, fundamentally understanding these macromolecular architecture changing influences these properties is of importance.

In this chapter, the different molecular architecture was firstly reviewed along with branching preparation technology. The available theories and methodologies for evaluating branching-containing materials are also discussed. Typical rheological behaviors of linear and branched polymers are also briefly described. The recent studies regarding high melt strength PPs are also reviewed and summarized.

2.2 Molecular Architecture

Altering molecular architectures plays an essential role in achieving desired polymer flow and mechanical properties. Knowing how molecular architecture influences the properties is critical to material scientists and engineers for better designing for a material with desirable properties. The chain architecture can generally be categorized into three types: linear, branched, and crosslinked. (Figure 1)

The linear polymer chain is composed of a backbone without branching and crosslinking. As the chain length is longer than a critical molecular weight (M_c), the chain is capable of entangling with surrounding chains; therefore, the viscosity of polymer will be significantly higher than the fluid composed of monomer units or chains shorter than M_c. The M_c is found to be two times the molecular weight between entanglements (M_e), which have been observed in a range of polymers with various chemistries [5, 6]. The viscosity (η) for an entangled polymer melt shows a universal dependence on molecular weight (M), which is $\eta \sim M^{3.4-3.6}$. The remarkable universality of this power law in a wide range of polymers suggests the existence of topological constraints by entanglements, dominating the viscoelasticity of polymers.
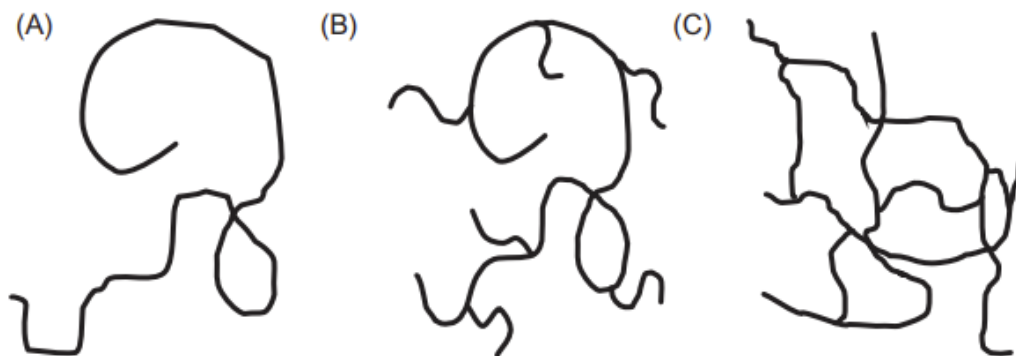
Figure 1. Three types of molecular architecture are (A) linear, (B) branched, and (C) cross-linked polymers [7]. Figure reprinted with permission from Elsevier (2018).

Branched polymers exhibit a linear main chain with branches grafting onto the backbone. The branching architecture can further categorize branched polymers, and some of the branching architectures are illustrated in Figure 2. Significant research efforts have been devoted to designing these molecular architectures via well-controlled polymerization. Various polymerization techniques have been implemented to design branching architecture, including atom-transfer polymerization, reversible addition-fragmentation chain transfer, ring-opening metathesis polymerization, anion polymerization, and cationic polymerization [8-12].

Although enormous chemistry synthesis methods have been proposed to prepare well-designed molecular architectures for achieving preferable polymer physicochemical properties, these procedures are usually very time-consuming and expensive. As a result, it is challenging to implement these methods into practical industrial applications. The post-reactor process, which incorporates a coupling agent to introduce branching reaction, has been created to economically prepare the branching structure. In particular, it has been

8

reported that the peroxide-initiated grafting process [13, 14], electron beam irradiation [15, 16], and gamma irradiation [16, 17] can successfully introduce LCB on the polymer backbone.

With branching junction points continuously growing, a giant three-dimensional network structure will be eventually created. Crosslinked polymer usually involves covalent or ionic bonds holding segments together, forming a mechanically stable network structure [18]. These intermolecular forces are strong bonding compared to secondary bonding such as hydrogen bonding and van der Waals forces; herein, these polymers are not softened with heating. Therefore, the heavily crosslinked polymer is commonly termed thermosetting polymers. The critical difference between branched and crosslinked polymer is that branched polymer will eventually loosen if a significantly longer relaxation time is given. The physical properties of a crosslinked polymers are strongly dependent on their crosslinking density. Experimental and simulation studies have found that ultimate tensile strength increases while ultimate strain decreases with increasing crosslinking density [19].
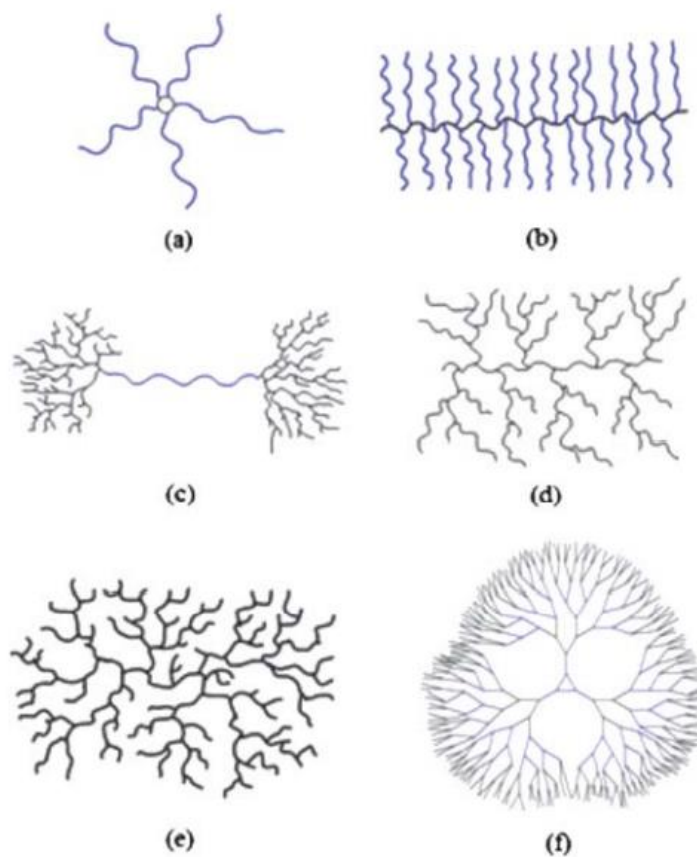
Figure 2. Illustration of branching architecture (a) Star (b) Bottlebrush (c) Pom-pom (d) Dendrigraft (e) highly/gyper-branched (f) dendrimer [10]. Figure reprinted with permission from Royal Society of Chemistry (2010).

2.3 Methodologies for Branching Characterization

The physical properties of a polymer are closely related to molecular architectures, and extensive research work has incorporated branching/crosslinking structures to adjust polymers' flow and mechanical properties [8, 9, 20-23]. Therefore, it is of particular importance and of interest to evaluate molecular architecture and branching characteristics via available techniques. However, because of the complexity of branching architecture, i.e., branching points, branching position, branching length, it is still a challenge for

polymer scientists to describe the branching characteristic and features fully and determine how these parameters interplay with the material properties. Moreover, the definition of a "long" branch varies with the chosen instrument since each instrument's working theories and limitations are different, making defining and interpreting from work to work even more difficult.

2.3.1 ^{13}C Nuclear Magnetic Resonance Spectroscopy

^{13}C Nuclear Magnetic Resonance Spectroscopy (NMR) has been utilized as a versatile tool for exploring chemical structure, end group analyses, and side-chain dynamics of polymeric materials [24]. Extensive research studies have used ^{13}C NMR as a quantitative characterization tool to evaluate the branching content in branched polymers [2, 25-28]. ^{13}C NMR defines LCB as a chain longer than six carbons [26, 29]. There are three ways to identify branching numbers by ^{13}C NMR: (1) signal of alpha carbon (C_α), (2) signal of branch carbon (C_{Br}), (3) combined signals of C_α, C_{Br}, and beta carbon (C_β) [27, 28]. Although ^{13}C NMR is an intrinsically direct quantitative method to quantify LCB content, it is necessary to combine with other technologies to provide the whole picture of branching architecture because of its low sensitivity to low level of branching content (<0.1 branch per 1000 C) and tedious efforts required to resolve signal overlapping issues for samples containing C4-C6 copolymer [2, 24, 27, 28].

2.3.2 Gel Permeation Chromatography

Gel Permeation Chromatography (GPC) with triple detectors (refraction index, viscometer, and light scattering) is a powerful tool to obtain information about the molecular weight distribution. In addition, the determination of branching density by GPC coupled with viscometer and light scattering detector has been well demonstrated [30-32]. In a dilute solution, the branched polymer is more compact to a linear one of the same molecular weight. The branched polymers with a smaller molecular size tends to have lower resistance to the solvent, reducing its intrinsic viscosity and radius gyration; therefore, the branching degree information can be obtained if a linear reference is given [32]. The contraction factor (**g** or **g'**) is

$$\mathbf{g} = \left(\frac{< R_g^2 >_{\text{branched}}}{< R_g^2 >_{\text{linear}}} \right) \tag{1}$$

$$\mathbf{g'} = \left(\frac{[\eta]_{\text{branched}}}{[\eta]_{linear}} \right) \tag{2}$$

Where **g** and **g'** are the contraction factors obtained from a light scattering detector and a viscometer, respectively, $< R_g^2 >$ is the radius of gyration, and $[\eta]$ is the intrinsic viscosity.

One of the advantages is that GPC can provide the LCB degree as a function of molecular weight, while NMR and rheology measure the average branching characteristics in the samples. However, if the branching degree is low, the divergence from the linear reference line is slight. As a result, the signal-to-noise ratio becomes too high to give reliable branching degree information [29, 33]. It is essential to note that the

difference between long and short-chain branches is not clearly defined in GPC measurements.

2.3.3 Rheology

Rheology is a study concerning a material's response to applied stress or strain. The melt rheological behavior of entangled polymer is strongly influenced by several molecular structure parameters, including molecular architecture, molecular weight, molecular weight distribution, and level of branching degree [34]. Rheology is considered an indirect and qualitative method to characterize LCB features. However, the rheological method is one of the most sensitive methods to detect a low level of LCB compared to NMR and GPC [29, 33]. Rheology defines LCB as a branch longer than M_e. The sufficient long branches can entangle with surrounding chains, increasing entanglement density and influencing their flow properties. Branches shorter than entanglement molecular weight has been found to have little impact on the linear rheological properties of a polymer [2]. Due to the different definitions of LCB to NMR, it has been found that the branching degree determined by NMR does not always correspond to its rheological behavior [29].

The presence of LCB in a molten polymer typically shows the following characteristics: (1) pronounced shear-thinning behavior because branches tend to disentangle under higher shear rate (2) higher zero-shear viscosity because of higher entanglement density (3) increase in strain-hardening degree in an extensional flow viscosity measurement [33, 35]. Moreover, due to additional relaxation modes of branches, LCB-containing polymer is thermorheological complex, which means multiple

activation energies exhibited in the LCB systems [36, 37]. Rheology is of importance due to its close relation to processing. Therefore, extensive research has focused on implementing rheological analyses combined with GPC and/or NMR to characterize LCB polymers.

2.4 High Melt Strength Polypropylene

Commercially available PPs produced by coordination polymerization mechanisms with Ziegler-Natta or metallocene catalyst usually exhibit linear structure with a rare branching structure. The linear structure of PP results in its low melt strength and insignificant strain-hardening behavior, which is of importance in extensional-flow-dominated applications, such as thermoforming, blow molding, and foaming. Recent advances in enhancing the melt strength of PP are reviewed and summarized below.

2.4.1 LCB Incorporation

Introducing LCB onto the PP backbone has been considered one of the most efficient ways to improve the melt strength of PP. The preparation of LCB containing PP can be categorized into two groups: (1) in situ polymerization and (2) post-modifying process initiated by high energy irradiation or peroxide [38-42]. Ye and Zhu synthesized comb-like branched PP using binary iron and zirconium single-site catalysts. The as-synthesized PP exhibits an isotactic backbone grafted with atactic branches. The atactic PP macromonomer was first generated by the iron catalyst, followed by copolymerization of the atactic PP macromonomer and propylene monomer [43]. Langston et al. presented another route to prepare LCB PP with metallocene catalyst combined with a T-reagent, p-

(3-butenyl)styrene. T-agent acts as a comonomer and chain transfer agent, contributing to LCB formation on the PP backbone [44]. More recently, LCB PP is successfully synthesized by Ziegler-Natta Catalyst, assisted with ω-alkenylmethyldichlorosilane in the presence of hydrogen. Enhancements in shear-thinning and strain-hardening degree were observed in the in situ synthesized LCB PP [41, 45].

Besides in situ polymerization for LCB PP preparation, the post-modifying process is used to introduce LCB onto the PP backbone to improve the PP's processibility in elongational flow-dominated applications. UV irradiation, gamma irradiation, electron beam, and peroxide have been used to generate radicals in PP systems for subsequent branching reactions assisted with a bi-functional coupling agent [39, 41, 43-47]. Although the post-modifying process is considered more applicable for industries, the involved reactions and the produced molecular structures are complicated due to the simultaneous branching, degradation, and crosslinking reactions.

Tian et al. prepared LCB PP by melt grafting reaction with an addition of peroxide and polyfunctional monomer, pentaerythritol triacrylate [35]. Without polyfunctional monomer incorporation, a decrease in viscosity was found, suggesting degradation of PP. As polyfunctional concentration increases, the evident shear-shearing and deviation from terminal behaviors indicate LCB formation. Other types of peroxide and polyfunctional monomers were also used for preparing LCB PP. Auhl et al. utilized electron beam irradiation for PP macroradical generation to form LCB PP, followed by an investigation of their rheological properties [33]. A shift to a lower phase angle with an increase in irradiation dose at the same complex modulus is attributed to LCB formation. Moreover,

the irradiated PPs with LCB exhibited pronounced strain-hardening behaviors in comparison to non-irradiated PP. Preparation of LCB PP via UV irradiation and a coagent has been recently reported. Increased complex viscosity, lower phase angle, and lower intrinsic viscosity suggested the successful LCB incorporation [39, 46].

2.4.2 Crosslinking

Some studies suggest crosslinking can improve PP's melt strength, thermal and chemical resistance [48-50]. Liu et al. prepared crosslinked PP in a twin-screw extruder with the addition of peroxide, styrene, and vinyl trimethoxysilane (VTMS) [49]. The gel content increased with peroxide and VTMS and reached the maximum of 40%. The melt strength increases and then decreases with further increasing the gel content. The foaming ability of VTMS crosslinked PP was significantly improved compared to the neat PP. PP was crosslinked via irradiation with Co-60 γ-rays with a polyfunctional monomer addition in another work [50]. The gel content was up to around 50%, and the foamability and cell structures were significantly improved. However, due to the uneasy control of the crosslinking process and crosslinking density, the fundamental understanding of this process to improve the melt strength of PP is still needed.

2.4.3 Filler Incorporation

Incorporating fillers and nanomaterials has been utilized to tune the rheological behaviors and functionalities of polymers. Extensive research has found that addition of nanofiller could enhance the strain-hardening degree, melt strength, and formability of PP.

16

The inclusion fillers include nano clay, multi-walled carbon nanotube, nanofibril, etc. [51-53]. Increases in melt strength and strain-hardening are usually attributed to more extended relaxation modes introduced by filler incorporation [51]. The nanofiller retards the relaxation process of polymer chains, creating a higher energy activation for chain motions, thereby the more solid-like behavior of polymer nanocomposites [54]. Moreover, adding a compatibilizer helps further enhance the strain-hardening degree due to the formation of three-dimensional networks with strong interaction between fillers and the PP matrix. However, it has been noted that achieving well-dispersed and good adhesion between filler and matrix are still very challenging. The expense of the filler is also a concern for applying this method to enhance the melt strength of PP.

CHAPTER III

QUANTIFICATION OF LONG-CHAIN BRANCHING CONTENT IN

POLYPROPYLENE*

In this chapter, a new methodology is proposed to quantify LCB molar fraction in PP systems. GPC and small amplitude oscillatory shear were employed to quantify LCB molar fraction and its influence on rheology in PP. The dependency of zero-shear viscosity (η_0) on the weight-average molecular weight allows for a reliable estimation of η_0 of LCB component in PP. Logarithmic mixing rule has been applied to obtain LCB molar fraction in each LCB-containing PP system. Quantitative assessment of how the LCB molar fraction influences PP rheological behavior is proposed.

3.1 Introduction

It has long been recognized that LCB structure in polymers cannot be definitively characterized using currently available analytical methods. Nuclear magnetic resonance (NMR) spectroscopy is beneficial for quantifying the number of branching points [55-57]. However, the length of the branches, especially those longer than six carbon chains, is indistinguishable from the spectra. Furthermore, Shroff and Mavridis have demonstrated that high branching numbers determined by NMR do not correlate with rheological

measurements, where LCB is defined as a chain longer than the entanglement molecular weight (M_e) of a given polymer [29]. Gel permeation chromatography (GPC) coupled with triple-detector (infrared detector, viscometer, and multi-angle laser light scattering) provides an alternative method for assessing branching extent as a function of molecular weight (MW) [58, 59]. Given the same MW, molecules with branches tend to possess a smaller radius of gyration, which corresponds to a lower intrinsic viscosity [η]. The ratio of the mean-square radius of gyration (or [η]) between branched and linear polymers becomes less than one. It has been noted that the difference between branched and linear polymers can be indistinguishably small if the branched polymers contain only a few branches per molecule [60]. That is, the LCB content measured using GPC for lightly branched polymers may be unreliable.

Rheological measurement is an indirect but more sensitive method to characterize LCB compared to NMR and GPC [29, 60]. LCB leads to higher elasticity, which produces higher storage modulus (G'), higher zero-shear viscosity (η_0), and lower phase angle (δ). Since LCB are prone to disentanglement under shear, polymers containing LCB exhibit a more substantial shear-thinning effect in comparison to linear samples [14, 61-63]. Furthermore, with respect to thermorheological behaviors, polymers containing LCB fractions exhibit higher activation energy compared to their linear polymer counterpart [36, 64]. Stadler et al. studied the thermorheological complexity of various polyethylene (PE) systems and determined that there is more than one activation energy barrier for the LCB containing PE with the lower activation energy component to be similar to that of

the linear PE. Multiple activation energy characteristics in a LCB containing polymer are indicative of their thermorheologically complex behavior [37].

Apart from the previously mentioned qualitative rheological methods, quantitative rheological methods have also been proposed to describe LCB structure and predict the LCB content of polymers. By considering a LCB PP as a blend consisting of LCB and linear chains, Tsenoglou and Gotsis calculated branching fraction based on different η_0 dependency between LCB and linear PPs by assuming that there is only one branch per backbone and that every branch carries the same MW equal to half of a linear chain [65]. The branching fraction and η_0 were observed to correlate well with an increasing amount of peroxydicarbonate initiator that promotes LCB formation. One drawback of this method is that the zero-shear viscosity of the modified polymer has to be higher than the linear polymer to be able to estimate LCB content, which significantly limits the applicability of this method.

Following the same idea and similar assumptions, Tian et al. adopted the relaxation time spectra instead of η_0 to determine both the LCB length and the fraction of branched chains by assuming one branching point per backbone in the PP matrix [14]. It estimated that the LCB branch length was approximately one-third of the main chain. Although the above approaches seem to have achieved a quantitative assessment of branching structure in an unknown LCB-containing polymer, the assumptions involved are unrealistic. It is highly likely that more than one branch per molecule may form, especially with an increasing amount of coupling agent incorporated. Additionally, detectable drops in MW were found in both of the above studies, suggesting partial degradation of polymer chains

has occurred. Since η_0 and the relaxation time is greatly dependent on MW, the emerged low MW fraction in their LCB-PP renders uncertainties in the usefulness of the above-proposed methodologies [66].

The Coupling model introduced by Ngai has been applied to account for the relaxation behaviors of a wide array of complex systems, including polymer melts, glasses, ionic conductors, semiconductors, etc. [67-69]. In linear monodispersed polymer melts, the relaxation processes of each chain are slowed down by coupling because of entanglements and other physical interactions among the neighboring chains. This process occurs in a system with relaxation time higher than the characteristic time or cross-over time, t_c, which is a temperature-independent parameter determined by the complex environment [67-69]. In a melt state where the coupling effect is dominated by entanglement, the crossover time is usually referred to as the Rouse time. Ngai and his coworkers have shown that the temperature dependence in 3-arm star polyisoprene (PI) is stronger than in linear PI and described the coupling strength using the Coupling parameter (n). A higher n was found for 3-arm star PI, which also exhibited higher activation energy [70].

The objective of this work is to establish a more reliable methodology whereby a low level of LCB molar fraction can be detected and quantified based on fundamental physics and can hence be adopted for determining the role(s) of LCB on influencing physical, mechanical, and rheological behaviors of LCB-containing polymers. In this study, the rheological behaviors of a series of model LCB-containing PP (LCB-PP) systems modified by an increasing amount of coupling agent were first qualitatively

21

characterized. Subsequently, a refined quantification methodology based on the one proposed by Tsenoglou and Gotsis is introduced. The significance of the present study for the quantification of LCB molar fraction in PP and for the development of high melt-strength PP is also discussed.

3.2 Materials and Methods

3.2.1 Materials

Model LCB-PP samples, which were modified with an increasing amount of proprietary coupling agent [71] using twin-screw extrusion with temperature setting at 210–250 °C, were supplied by Braskem, USA. Table 1 records the details of the composition of the model systems. For consistency and clarity in comparing among the PP systems investigated in this study, the number shown with each label stands for the determined LCB molar fraction in LCB-PP obtained through the proposed methodology. To minimize degradation, 0.1 wt% of a commercial antioxidant was added in LCB-PPs. Additionally, BRPP-19 was diluted with linear PP (LPP-a) at three different weight ratios (75/25, 50/50, 25/75 w/w) to obtain BL-14, BL-10, and BL-5 using a System 40 Haake mixer at 20 rpm and 200 °C for 5 min.

To demonstrate the industrial relevance of our approach, a commercially available high melt strength PP (CPP-24, Daploy^{TM} WB140HMS, Borealis, USA) and another linear PP (LPP-b) with similar MW to CPP-24 were also blended and characterized to show how a controlled amount of LCB can be utilized to tailor the rheological behavior of PP, even in commercial systems.

Table 1. Designation of the model LCB-PP samples having different amounts of coupling agent incorporated.

Sample label	Coupling agent (wt%)
LPP-a	0
BRPP-5	2
BRPP-13	5
BRPP-19	8

3.2.2 Characterization

The molecular characteristics of each sample were determined by a high-temperature GPC (Polymer Char GPC-IR®) equipped with an infrared (IR) detector (IR5 MCT) and a viscometer. GPC measurements using narrow MWD Polystyrene standards (Polymer Char Narrow PS standards) for calibration were performed by Formosa Plastics, USA. The GPC was carried out at 145 °C with an eluent of 1, 2, 4-triclorobenzene. The 200 µL sample solution with a concentration of 1 mg/mL and filtered before injected into the GPC system. The flow rate was set to 1.0 ml/min.

Small amplitude oscillatory shear (SAOS) was performed in a strain-controlled rotational rheometer ARES-G2 (TA instruments) using a 25 mm parallel plate geometry under a nitrogen atmosphere. Linear viscoelastic region (LVR) was determined by a strain sweep, and a strain of 5% was used in the SAOS study. A time sweep was used to check for possible thermal degradation or structural change during the experiments. Changes in storage and loss modulus below 5% are considered acceptable and assumed to be thermally stable. All samples were thermally stable for at least 2 hours, which was more than the time required for all of the rheological characterizations. The test frequency range was chosen to be 0.01–100 rad/s, and the sample gaps were set at 1.0 mm. The creep

experiment was carried out at a constant shear stress of 5 Pa for 3600 s. A stress control step was performed before each creep test for optimizing motor control parameters. This step allows ARES-G2 to conduct stress-controlled experiments.

3.3 Results and Discussion

3.3.1 Branching Reaction

The model LCB-PP system prepared in this study is quite unique and is ideal for the validation of the proposed methodology in determining LCB molar fraction in PP. The coupling agent used in this study is a proprietary polymeric coupling agent containing difunctional reactive groups with a generic structure shown in Figure 3 [71]. An azide-containing functional group residing on one end of the molecule can generate free radicals during compounding. The other end of the molecule can be another reactive group containing vinyl group, which can react with excess free radicals and minimize chain scission in the PP main chain. The polymeric mid-segment is designed to achieve the best compatibility with the PP matrix. Consequently, the coupling agent used in this study is effective for homogeneous LCB grafting reaction with minimal impact to degradation and gel formation in PP.

To better describe the possible branching reactions in the preparation of the model LCB-PP, the proposed branching reaction is shown in Figure 3. Thermal decomposition of an azide group in the coupling agent generates a singlet/triplet nitrene after the release of nitrogen gas. The singlet nitrene group is capable of chain insertion into the PP chain, while the triplet nitrene can extract a hydrogen atom from the PP backbone, forming a PP

24

macroradical for subsequent branching reactions. After nitrenes are grafted onto PP main chains, the vinyl functional group on the other end of the coupling agent can react with macroradicals to undergo chain extension. Moreover, the vinyl group on the coupling agent can stabilize the macroradicals soon after the nitrenes attack on PP chains. This dramatically minimizes the β scission of the PP backbone, thus, preventing the generation of low MW PP. Finally, when two macroradicals recombine in the melt, they form LCB-PP structures.

3.3.2 GPC and Rheological analyses

The GPC results are tabulated in Table 2. The weight-average molecular weight (M_w), number-average molecular weight (M_n), molecular weight distribution (MWD) and amount of mass recovery, i.e., gel content, are reported for each model system. The increases in MW and MWD with an increasing amount of coupling agent incorporation are due to the LCB formation in the high MW regime (Figure 4). It is noted that the mean MWD peaks for the LPP-a and BRPPs curves remain unchanged after the LCB grafting. Although the branching reaction introduces LCB, it may also produce gel particles as a by-product. As shown, all model LCB-PP systems contain less than 4 wt% of gel particles, which is generally found not to influence the SAOS study [72]. As shown in Figure 4, the emerged shoulders of BRPPs in the high MW regime correspond with the region where the intrinsic viscosities start to deviate from that of linear PP. The observed reduction of intrinsic viscosity is indicative of the formation of the branched structure in PP, leading to a smaller molecular size in comparison to a linear PP with the same MW.

Coupling agent
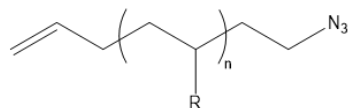
Radical formation

(1) singlet   (2) triplet
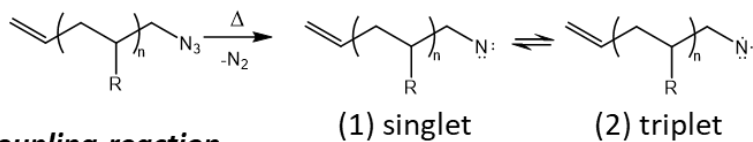
Self-coupling reaction

Branching reaction

(1)

(2a)

PP'   PP'•

(2b)

PP''   PP''•

(2c)

PP'•
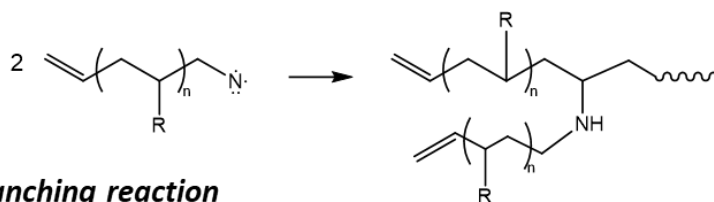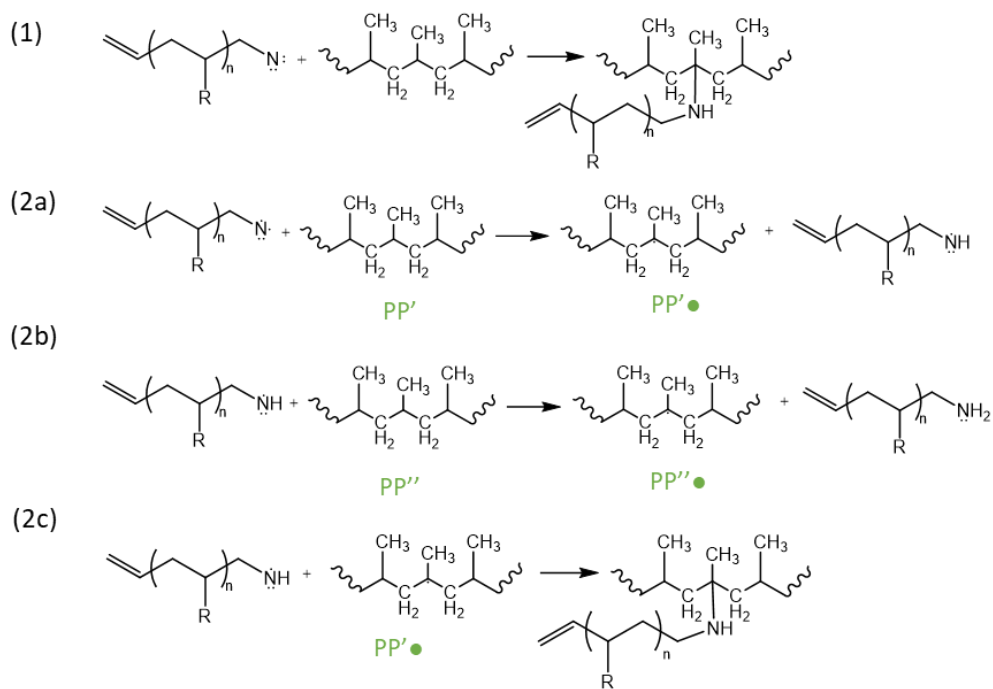
Figure 3. Branching reaction scheme.

26

Table 2. Molecular weight information of the model PP and LCB-PP systems obtained from GPC-IR coupled with a viscometer.

Sample	M_w (g/mol)	M_n (g/mol)	MWD	Mass recovery (wt%)
LPP-a	1.9×10^5	3.4×10^4	5.6	98
BRPP-5	2.0×10^5	3.4×10^4	6.0	99
BRPP-13	2.4×10^5	4.0×10^4	5.9	97
BRPP-19	2.7×10^5	4.1×10^4	6.7	96
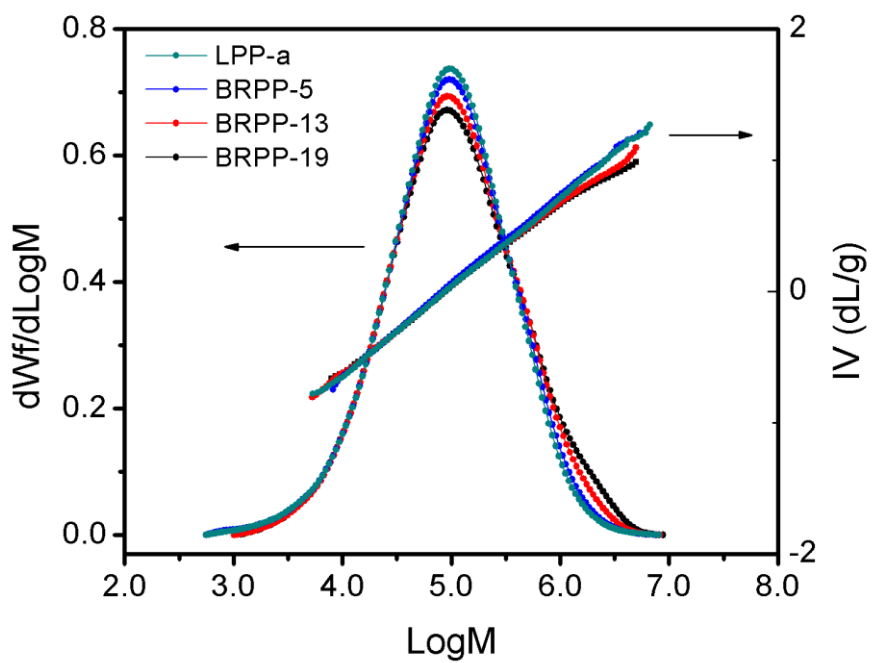
Figure 4. Plots of weight fraction and intrinsic viscosity against fractionated molecular weight.

27

The number of branching points per molecule (**B**) for randomly formed branched polymers with similar branch lengths can be estimated from the Zimm–Stockmayer equation [73],

$$\mathbf{g}' = \left(\frac{[\eta]_{\text{branch}}}{[\eta]_{linear}}\right)^{\frac{1}{\epsilon}} = \left[\left(1 + \frac{\mathbf{B}}{7}\right)^{0.5} + \frac{4\mathbf{B}}{9\pi}\right]^{-0.5} \tag{3}$$

where **g'** is the chain contraction factor calculated from the intrinsic viscosities of the branched and linear PP, and ϵ is assumed to be 0.5 for a non-free drain star-like polymer [73]. The **g'** factor of each model system is plotted as a function of MW (Figure 5). The average values of **g'** factor and **B** in the model LCB-PPs are listed in Table 3. As expected, the **g** is nearly independent of MW and decreases with an increasing amount of the coupling agent incorporated. A nearly constant branching number per molecular (**g'**) for each model system in the MW ranging between 5.0×10^5 and 1.0×10^7 g/mol suggests that the coupling agent was well-dispersed in PP matrix during compounding and branching reaction. The increase in number of branching per molecule from 0.4 to 3.1 is due to the higher concentration of coupling agents introduced in PP. The GPC combined with the intrinsic viscosity analyses suggests that the branched structure has been successfully generated in the model systems. It should be noted that no detectable additional low MW PP fraction is found in the model LCB-PP systems. This implies that the coupling agent utilized in this study is effective in generating branches without causing a noticeable reduction in PP MW.
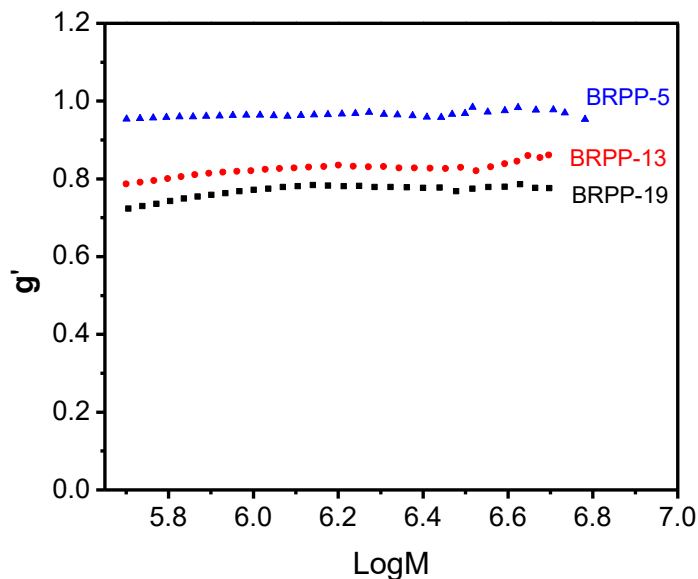
Figure 5. The values of **g'** as a function of MW in LCB-PPs.

Table 3. The average g factor and the calculated B.

Sample	**g** factor	**B**
BRPP-5	0.96 ± 0.02	0.4
BRPP-13	0.83 ± 0.01	2.2
BRPP-19	0.76 ± 0.01	3.1

For a branched chain to effectively achieve cooperative motion with the surrounding chains, thereby retarding the relaxation process and influencing the flow behavior in a polymer, the branched chain length should exceed the M_e [74]. Rheological property measurements were undertaken to closely examine the linear viscoelastic properties of the model LCB-PPs. Storage modulus (G') represents the ability of a polymer to store energy, and loss modulus (G'') refers to its ability to dissipate energy as heat after applying strain or force. Figure 6 shows a double logarithmic plot of G'-angular frequency

covering the frequency range of 0.01–100 rad/s at 190 °C for each model LCB-PP system. The magnitude of G' increases at low frequencies with an increasing amount of coupling agent, indicating that most of the branches formed are long enough to influence the entanglement density and viscoelasticity of PP.
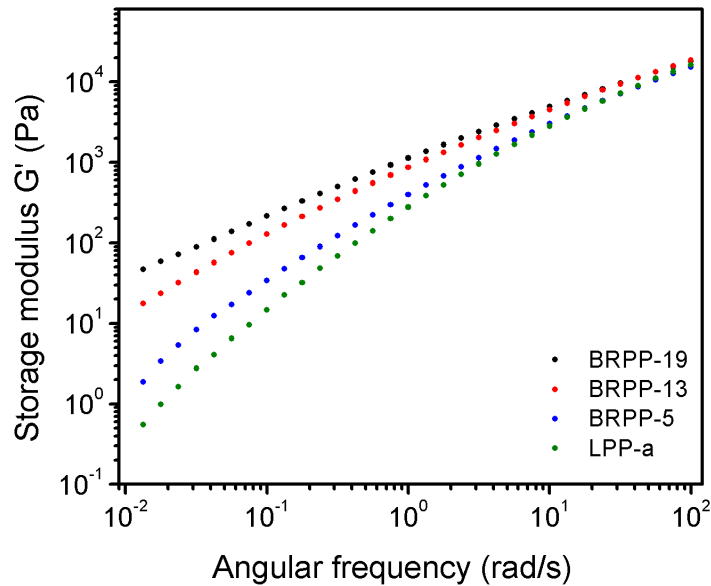
Figure 6. Linear viscoelastic response of linear and LCB-PPs. Storage modulus (G') is shown as a function of angular frequency.

The van Gurp-Palmen plot (vGP plot), which correlates the phase angle (δ) with the complex modulus (G*), was further constructed to determine their subtle relaxation behavioral changes due to the formation of LCB in PP. The δ is defined as the arctangent of the ratio of G'' to G', a delay between the applied deformation and the responsive stress. It signifies relative liquid-like or solid-like characteristics of a material. Trinkle et al. have demonstrated that the vGP plot can differentiate subtle changes in polymeric molecular

30

structure and validate the time-temperature superposition principle in materials [75, 76]. The curves in the vGP plots are only superimposable if the relaxation processes are the same, and δ will be a single value for a given G^*. The vGP plots for PPs with increasing LCB molar fraction are shown in Figure 7. For BRPPs, their clear departures from the linear PP curve are observed, suggesting that the presence of LCB significantly contributes to longer relaxation times and higher elasticity at 190 °C, especially in the low-frequency region. The phase angle of LPP-a reaches the terminal value of 90° as the test frequency reduces to 0.01 rad/s; whereas, BRPP-19 with the highest LCB molar fraction is still far from reaching its terminal value. This implies that BRPPs possess a significantly longer relaxation time than linear PP. Additionally, the decrease in δ with an increase in LCB molar fraction suggests that stronger molecular cooperativity in LCB-PPs leads to a more solid-like characteristic.

From both the GPC and rheological measurements, it is confirmed that the branched structure has been successfully introduced onto linear PP by incorporating the coupling agent and that the branch length of LCB is long enough to strongly retard the relaxation process in PP.
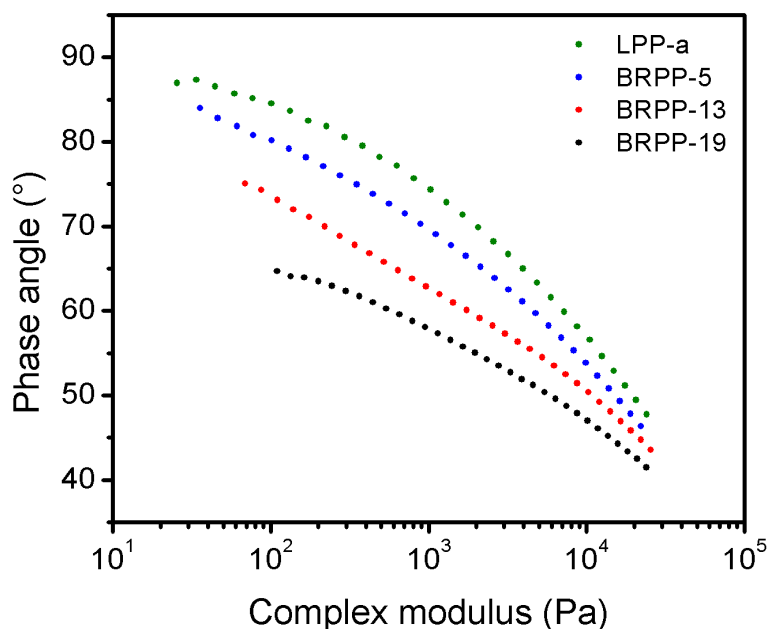
Figure 7. The van Gurp-Palmen plots of PP with increasing LCB molar fraction measured at 190 °C.

3.3.3 Quantitative LCB Molar Fraction Determination

As mentioned earlier, the quantification of the LCB molar fraction is considerably challenging, especially for post-reactor modified LCB-PPs because of their potentially complex LCB architecture. It is understood that the exact molecular architecture in the LCB-PP produced in this study cannot be determined. Nevertheless, it is still of importance to be able to quantitatively determine LCB molar fraction for a fundamental understanding of the structure-property relationship in LCB-containing polymers. Herein, we propose a new approach to assess the LCB molar fraction in PP.

To carry out quantitative analysis, two reasonable assumptions are made. The first assumption treats the BRPP model systems as homogeneous blends of both linear and

32

LCB with increasing amounts of LCB in LPP-a. As shown in Figure 4, the dominant peaks of the MW curves of BRPPs are located at the same MW position as that for LPP-a. Moreover, all the intrinsic viscosity values below log M = 5.5 merge with that of LPP-a, suggesting that most LPP-a chains do not react with the coupling agent and serve as the dominant phase in the matrix. It is conceivable that a small amount of low MW PP fraction might also form and cannot be detected by GPC in this regime, which should not affect the rheological behavior analysis to be presented below. As shown in Figure 8, there is no drop in complex viscosity in all BRPPs, suggesting that the potential presence of low MW PP has a negligible effect on the rheological property compared to that due to LCB. The second assumption considers that only simple and self-similar branches are formed in BRPPs rather than densely grafted branching structures, such as comb-like, tree-like, and pom-pom branching. Since the branch number estimated from GPC ranges from 0.4 to 3.1 per molecule, it is reasonable to consider that the LCB in BRPPs forms simple and self-similar branches in the main chain.
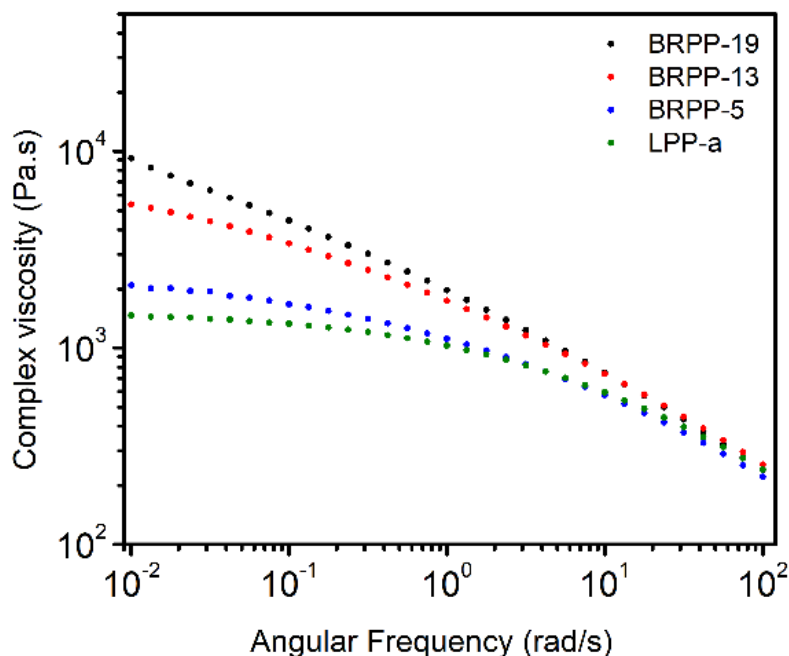
Figure 8. Complex viscosity as a function of angular frequency for BRPPs

Logarithmic mixing rule

Several research efforts have concluded that η_0 is one of the most sensitive parameters to detect the presence of LCB because its values significantly depend on the LCB content, branch length and the MW of the entire branching species [16, 77-79]. Therefore, the η_0 has been used to be a representative parameter to describe the LCB effect and to semi-quantify the LCB content. Other than η_0, the flow activation energy term has also been commonly utilized to describe LCB effects on thermorheological complexity in the LCB containing polymers [37, 64, 78]. The higher flow activation energy in LCB-PP implies that the intrinsic resistance for it to flow is higher than that of

34

linear PP, thereby reflecting in the higher η_0 of LCB-PP. The relationship between flow

activation energy and η_0 follows Arrhenius equation and can be described by

$$\frac{1}{\eta_0} = A \exp\left(-\frac{\Delta E}{RT}\right) \qquad (4)$$

where A is a constant, ΔE is the flow activation energy, R is the Boltzmann

constant, and T is the absolute temperature. By assuming that (1) the two components are

miscible, (2) there is no volume change during the blending process, and (3) the flow

activation energy values are additive between two different polymer structures, the flow

activation energy for a binary blend system consisting of x molar fraction for the first

component and (1-x) molar fraction for the second component can be calculated as follow:

$$\Delta E_{blend} = x\Delta E_1 + (1-x)\Delta E_2 \qquad (5),$$

where ΔE_{blend}, ΔE_1 and ΔE_2 are flow activation energies of blend, the first

component, and the second component, respectively. The activation energy in Equation

(3) can be replaced by η_0 using Equation (2), which leads to

$$\eta_{0,blend} = \left(\eta_{0,LCB}\right)^x \left(\eta_{0,linear}\right)^{1-x} \qquad (6),$$

where x is LCB molar fraction in the blend, $\eta_{0,blend}$ is the η_0 of the blend, $\eta_{0,LCB}$

is the η_0 of the LCB component and $\eta_{0,linear}$ is the η_0 of the linear component. Equation

(5) is the logarithmic mixing rule which has been widely applied to predict the viscosities

of the blends containing linear and lightly-grafted LCB polymers [14, 62, 65, 80-83]. It

should be noted that the linear and LCB components of the blended mixture need to be

miscible for Equation (5) to become valid [81, 84].

Determination of $\eta_{0,linear}$ and $\eta_{0.blend}$

      To apply the above blend mixing rule in this study, the accuracy of η_0 is critical in determining the LCB molar fraction. Therefore, the Cross equation and creep test were both used to obtain the values of η_0 for each model system. The Cross equation is used to predict η_0 by fitting the complex viscosity data using Equation (6),

$$\eta^* = \frac{\eta_0}{1 + (k\omega)^m} \tag{7},$$

where η^* is the complex viscosity, k is the Cross time constant, and m is the Cross shear-thinning index. The other method to obtain the values of η_0 is to conduct a creep test with a constant shear stress equal to 5 Pa and subsequently measure its steady-state viscosity. Figure 9 shows the values of η_0 obtained from the two methods, which are nearly the same as each other and are representative enough to describe the flow characteristics of each model LCB-PP system.
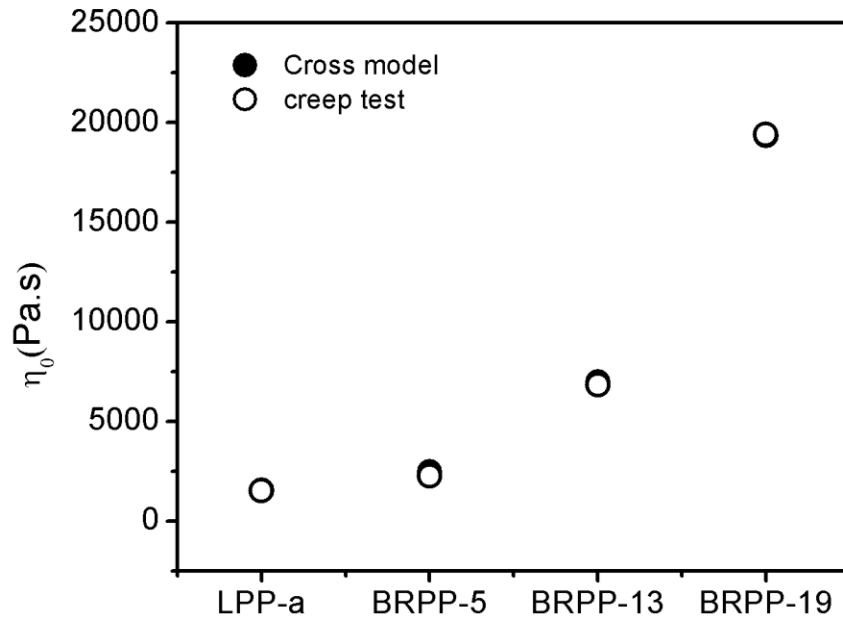
Figure 9. Comparison of η_0 obtained between the Cross model and the creep tests.

Determination of $\eta_{0,LCB}$ and LCB molar fraction

In a polymer melt, molecular chains longer than M_e are entangled and coupled with the surrounding chains [5, 74]. The relaxation process can only be accomplished through cooperative motions, which indicates that both intramolecular and intermolecular interactions should be considered. The Coupling model (CM) proposed by Ngai describes these molecular relaxation complexities using two physical parameters, a Coupling parameter n, representing the resistance against molecular mobility, and an apparent relaxation time τ^* [67]. In an entangled polymer, each chain is affected by the surrounding chains via entanglements when the time scale is longer than the environmental determined crossover time, t_c. Unlike a Rouse chain, it cannot relax without cooperativity from the

37

surrounding chains [67-70]. Stronger coupling effects are expected in the LCB system due to unfavorable processes of arm retraction before reptation [5]. Stronger coupling strength in LCB polymers explains their thermorheological complexity, higher resistance in flowing, and higher η_0. Based on Ngai's CM, the Coupling parameter n can be estimated with the following equation:

$$\eta_0 \propto M_w^{\frac{2}{1-n}} \tag{8}$$

Compared to n = 0.4 for linear systems, Ngai proposed that the Coupling parameter for LCB systems should be at least 0.7 to explain the stronger dependency of viscosity in LCB systems on MW [67], which is

$$\eta_{0,LCB} = KM_{w,LCB}{}^{6.5} \tag{9}$$

where K is a constant. The stronger η_0 dependency on LCB-containing polymers is found in many other studies, confirming the validity of Ngai's estimation [62, 85, 86]. Moreover, Lohse el. al. demonstrated that η_0 of the 3- and 4-arm branched polymers with short branch lengths were close to the linear reference line in their η_0-M_w log-log plots [62]. Consequently, LPP-a is assumed to reside at the intersection of two η_0-M_w lines of linear and LCB-PP systems and to act as a 3-arm branched PP with extremely short branches. Therefore, the $\eta_{0,LCB}$ can be estimated using Equation (7) if $M_{w,LCB}$ is known.

The prediction of $\eta_{0,LCB}$ is based on the relative M_W differences between LCB and linear components. Therefore, the M_W information obtained from the GPC-IR detector coupled with a viscometer should be adequate in this study [87]. The M_w of the LCB component can be estimated by subtracting the area between the LPP-a and BRPPs under the GPC curves (Figure 4) in the regime where the intrinsic viscosities of BRPPs deviate

from that of LPP-a. As shown in Figure 10 (a), considering BRPP-19 as an example, the MWD information of the LCB component is obtained by subtracting the curve of BRPP-19 from the curve of LPP-a in the region where log M > 5.5. Figure 10 (b) shows the MWD curves for BRPPs after the subtraction. The values of MW, LCB in PP for each system are listed in Table 4. It is noted that the MW of the LCB component increases slightly with the coupling agent content in PP. The increase in MW can be attributed to either more LCB is grafted onto the PP main chains, or a longer LCB branch length is formed for a given branch point per molecule. However, a more sophisticated GPC coupled with a triple detector may be needed for obtaining the actual MW,LCB because of uncertainties in their peak breadth and insensitivity in the high MW regime.
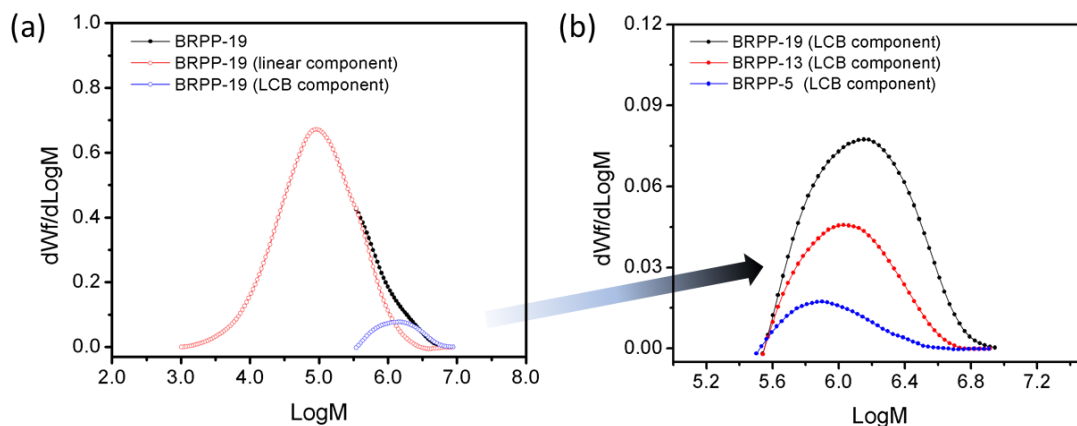
Figure 10. (a) The estimated LCB weight fraction in BRPP-19 is obtained by the curves subtraction between BRPP-19 and LPP-a in the high MW regime, which begins at log M = 5.5 (b) The MWD of LCB components in BRPPs.

Table 4. MW of LCB component, $\eta_{0,LCB}$ and LCB molar fraction.

Sample	MW,LCB (g/mol)	$\eta_{0,LCB}$ (Pa.s)	LCB molar fraction by the mixing rule (%)
LPP-a	n/a	n/a	0.0
BRPP-5	7.6×10^5	1.30×10^7	5.1
BRPP-13	1.1×10^6	1.29×10^8	13.4
BRPP-19	1.5×10^6	9.20×10^8	19.1

The determined values of $\eta_{0,LCB}$ are listed in Table 4. The calculated $\eta_{0,LCB}$ follows the same trend as that observed by Lohse et al. [62], suggesting that the estimation is reasonable. By applying the mixing rule shown in Equation (5), the LCB molar fraction in each system is calculated and shown in Table 4. The LCB molar fraction in BRPPs ranges from 5.1 to 19.1%. As expected, the LCB molar fraction in the model BRPPs increases with coupling agent content.

Experimental validation of the model

To confirm if the estimated LCB molar fraction in each model LCB-PP system is correct, BRPP-19 was intentionally blended with LPP-a to dilute the LCB molar fraction in BRPP-19 to a similar level as BRPP-5 and BRPP-13. The blending ratio and estimated LCB molar fraction of each new model LCB-PP system are listed in Table S2. BL-5 and BL-14 have LCB molar fraction close to BRPP-5 and BRPP-13, respectively. Therefore, it is expected that these blends would possess similar rheological properties as BRPP-5 and BRPP-13. Indeed, both the SAOS and vGP plots of BL-5 and BL-14 versus BRPP-5 and BRPP-13 show almost an exact match (Figure 11 and 7). This implies that the LCB molar fraction estimated by the proposed methodology is reasonable. The vGP plot shown

in Figure 12 gives a more complete description of their relaxation processes. As expected, the relaxation processes match well with each other for LCB-PP containing the same LCB molar fraction. With 10% LCB in PP, the plot of BL-10 falls in the middle between BL-5 and BL-14.

Table 5. The blending ratio of three blending systems and the estimated LCB fraction calculated by blending ratio.

Sample	BRPP-19 content (wt %)	LCB molar fraction by blending ratio (%)
BL-5	25	4.7
BL-10	50	9.5
BL-14	75	14.3
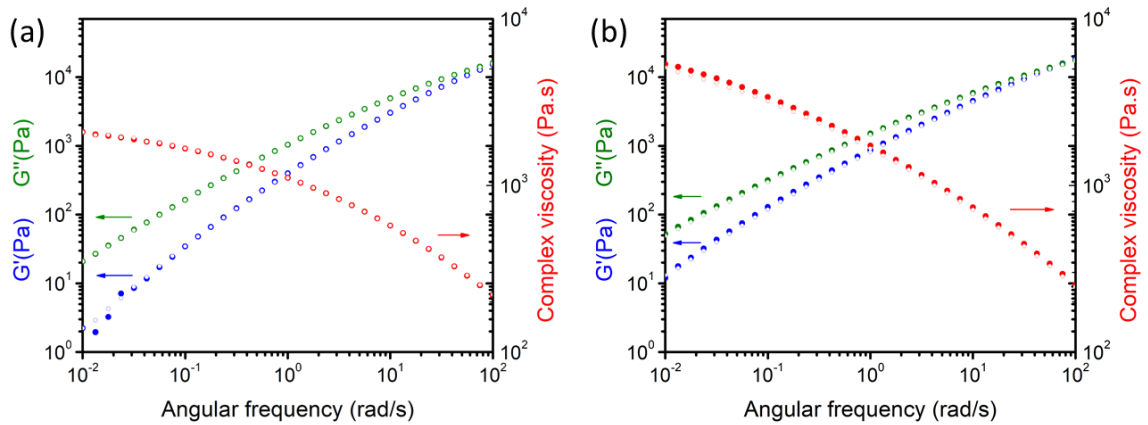
Figure 11. Small amplitude oscillatory shear measurement for LCB molar fraction in PP equal to (a) 5% and (b) 15%. Solid symbol: BRPP-5 and BRPP-13; open symbol: BL5 and BL14.
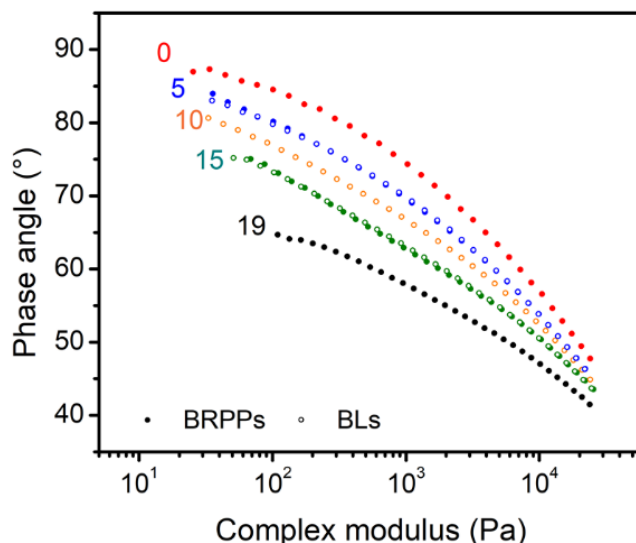
Figure 12. The vGP plots for BRPPs and the BLs. The number shown in the plot is the LCB molar fraction in each system.

The successful prediction of viscoelastic properties of the above blends suggests that the possible slight variation in the number of branching points and/or the length of branches in BRPP-5, BRPP-13, and BRPP-19 would not have a significant contribution to the flow behavior. On the other hand, for LCB with much denser branching structures, such as tree-like, branch-on-branch, and hyperbranched architectures, future research would still be needed to determine their characteristic η_0 dependencies on the M_w.

To further demonstrate the validity and usefulness of the proposed methodology in quantifying the LCB molar fraction in PPs and its universal applicability to other polymers, commercially available CPP-24 were melt-blended with LPP-b, which has similar MW and MWD to the linear polymer portion of the CPP-24. The detailed MW information of CPP-24 and LPP-b are listed in Table 6, and the MWD plot is shown in Figure 13. MW of LCB component in CPP-24 is 1.5×10^6 g/mol, similar to that in BRPP-

19. By carrying out the similar methodology as described above to determine the LCB molar fraction in CPP-24 and its diluted blends using LPP-b, the LCB molar fraction in each blend based on the blending ratio and the mixing rule are estimated and listed in Table 7. The slight discrepancy between the estimated LCB molar fraction based on the proposed methodology and the blending ratio can be partially attributed to the imperfect melt-mixing of the rather complex commercial CPP-24 system.

It is challenging to determine the LCB molar fraction solely based on the complex viscosity versus angular frequency plot (Figure 14) as a tool to compare between the two sets of PPs with the same LCB molar fraction, such as CPP-10 and BL-10 or CPP-14 and BRPP-13. The difficulties emerge from the dependency of η_0 on the MW of PP. The most effective way to semi-quantitatively analyze LCB content is to use the vGP plot [76, 85]. With the quantification of LCB molar fraction in PP obtained from the above-proposed methodology, it is possible to determine how the LCB molar fraction influences the rheological and relaxation behaviors in polymers. As shown in Figure 15, even with two different sets of model systems, the same LCB molar fraction in two different PP systems would give rise to nearly the same vGP plot, i.e., CPP-10 vs. BL-10 and CPP-14 vs. BRPP-13. The mismatch between BRPP-5 and CPP-5 is likely due to the differences in MW and MWD of their linear components, and too low of LCB molar fraction in both PP systems to strongly influence their relaxation behavior. Trinkle et al. have demonstrated that a wider MWD will shift the vGP plot curves to the left [75]. With increase in the LCB component, especially more than 10%, LCB component starts to dominate the overall relaxation behavior in PP systems.

43

Table 6. Molecular weight information on LPP-b and CPP-24.

Sample	Mw	MWD	MW of LCB component	Mass recovery
	(g/mol)		(g/mol)	(wt%)
LPP-b	2.2×105	5.3	n/a	100
CPP-24	3.7×105	6.3	1.5×106	95

Table 7. η_0 and LCB estimation in the CPPs.

Sample	η_0 (Pa.s)	LCB molar fraction (%)	
		Mixing rule	Blending ratio
LPP-b	2.58×10^3	0	-
CPP-5	3.26×10^3	4.6	5.9
CPP-10	8.70×10^3	9.8	11.8
CPP-14	1.52×10^4	14.2	17.7
CPP-24	4.81×10^4	23.6	-

44
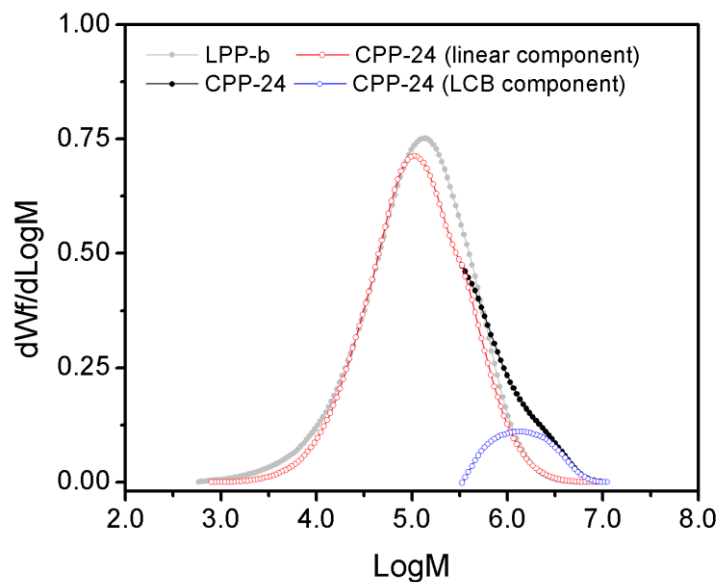
Figure 13. Molecular weight distribution of CPP-24, linear component of CPP-24, LCB component of CPP-24, and LPP-b.
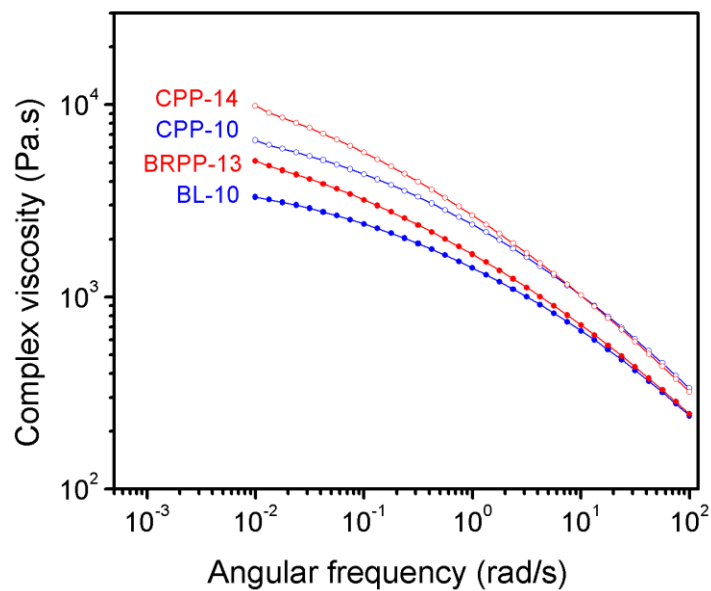
Figure 14. Complex viscosity as a function of angular frequency for two sets of LCB-PP with the same LCB contents.
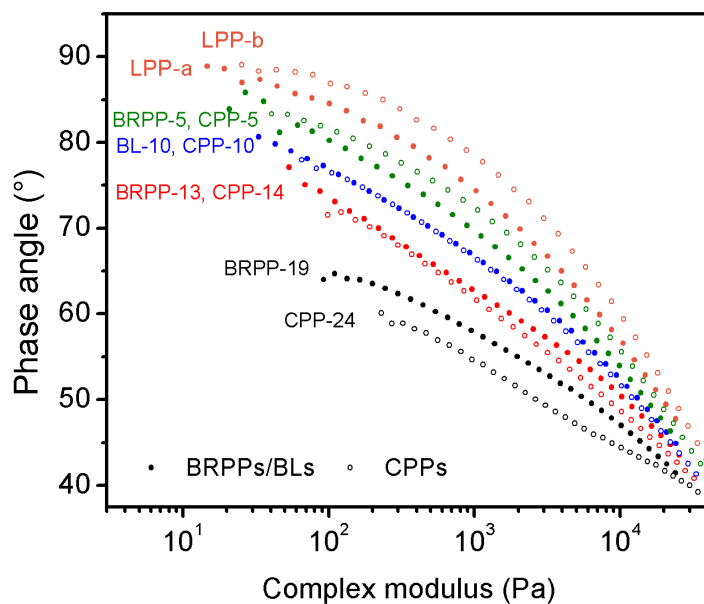
Figure 15. The vGP plots for two LCB-PP systems. Solid circle: LPP-a and BRPPs; open circle: LPP-b and CPPs.

The methodology proposed in this study used η_0 as a key parameter to determine the linear and LCB component in LCB-PP systems using GPC. Also, by taking into account the MW of linear and LCB components, it minimizes the influence of MW in LCB molar fraction determination. Therefore, LCB-PPs manufactured from different producers can still be compared quantitatively with the proposed methodology. According to our exhaustive literature review, there is no other known method that is capable of quantifying LCB molar fraction and predicting the rheological behavior from different producers.

Based on the present study, the proposed methodology can serve as a powerful tool for material selection in different applications and lays an essential foundation for the

46

fundamental study of LCB molar fraction effects on rheological and mechanical properties.

3.4 Conclusion

A set of model PP systems modified with an increasing amount of coupling agent was used as a set of model systems to investigate the LCB effect on rheological properties and to develop a methodology to quantify LCB in PP. These model systems contain no low MW fraction PP by-product and possess only loosely-grafted branching chains, which become ideal for the quantitative determination of LCB molar fraction in PPs. Most importantly, the proposed methodology can determine LCB molar fraction without a need to take into account the PP MW effect and the number of branching points per molecule. Additional work is still needed for the possible expansion of our proposed approach for determining LCB molar fraction in other LCB-containing polymers.

CHAPTER IV

LINEAR AND NONLINEAR VISCOELASTICITY OF POLYPROPYLENE

CONTAINING CROSSLINKED GELS

The dynamic viscoelastic and extensional flow behaviors of polypropylene (PP) with increased micron-sized gelled particles have been investigated. The results reveal that incorporating gelled particles can significantly enhance the PP melt storage and loss modulus, complex viscosity, and degree of strain hardening. The gelled particle, acting as a soft, deformable filler, exhibits a core-corona structure. The core is made of crosslinked PP, with the corona region consisting of chain loops, dangling chains, and strongly constrained PP matrix chains. The matrix chains begin to bridge globally between the adjacent gelled particles once the interparticle distance is shorter than the PP random coil size. The globally bridged structure, in turn, results in a gel-like behavior of the entire PP matrix. The present findings advance a fundamental understanding of the rheological behavior of polymeric systems containing self-similar soft particles for improving melt strength.

4.1 Introduction

Due to PP's linear structure and poor thermal stability, PP exhibits undesirable rheological characteristics, such as low melt strength and insufficient strain-hardening during processing [88]. These characteristics limit PP applications in blow molding, foaming, and thermoforming, where an elongational flow dominates. These

disadvantageous rheological characteristics of PP result in undesirable poor product qualities, such as inhomogeneous wall thickness, cell collapse, and film rupture.

To enhance PP processibility and physical properties, several post-reactor modifications have been proposed, such as blending with polyethylenes [89], filler incorporation [90], and grafting-crosslinking modification during processing [17, 88, 91-93]. Among these approaches, the grafting-crosslinking modification process is considered the most feasible and scalable to enhance the melt strength of PP due to its simple single-step process without incorporating relatively expensive fillers. The grafting-crosslinking modification can be categorized by the source of radical generation: gamma radiation [17], accelerated electron beam [91], and peroxide initiation [88, 92]. To enhance the grafting/crosslinking efficiency, a co-agent with multifunctional groups, also known as a polyfunctional monomer, is commonly used, such as divinylbenzene (DVB), peroxydicarbonates, and triallyl isocyanurate [17, 92, 93].

In the grafting-crosslinking modification of PP during processing, crosslinking, branching, and degradation usually happens simultaneously. The following reaction mechanism has been proposed for the grafting-crosslinking modification in PP [21, 94]. Free radicals generated by peroxide initiation or ionizing reaction, i.e., electron beam radiation, gamma radiation, etc., extract the hydrogen atoms on the PP backbone, forming macroradicals. The resultant PP macroradical attacks another PP backbone or macroradical to form crosslinking/branching structures. Incorporating a co-agent can stabilize the macroradicals to minimize β-scission and disproportionation reactions and increase the grafting/crosslinking efficiency. Due to the random termination of two

49

macroradicals, both LCB and cross-linked structures are simultaneously formed in the grafting-crosslinking modification in PP. Both structures are almost inseparable due to their near-identical chemical composition. Therefore, it is challenging to prevent gel formation during the branching reaction in PP [94, 95]. The lightly cross-linked gel particles can serve as a soft filler, and a low amount of gel content has been found to enhance thermal and chemical stability, impact strength, and cracking resistance, and melt strength [22, 96].

Several studies have observed the unique flow characteristics of nano-sized soft particles in comparison to impenetrable solid fillers [97-99]. Mackay and co-workers presented an all-polystyrene (PS) nanocomposite containing soft PS nanoparticles synthesized by intramolecular crosslinking a single PS molecular chain [100]. Chen et al. conducted coarse-grained molecular dynamic simulations to investigate the chain dynamics in the all-PS nanocomposite [97]. They found that, due to the inherent softness of PS nanoparticles, PS matrix chains can penetrate the PS nanoparticles, leading to a smooth density profile in the interfacial region. More recently, Shrestha et al. found that the diffusion rate of soft nanoparticles strongly depends on their internal crosslinking density and polymer matrix molecular weight [99]. The classical Stokes-Einstein hydrodynamic diffusion model fails to predict the observed reduction in diffusion rate of the soft nanoparticles. Considering the topological constraints by threading and dethreading of polymer matrix chains on the surface loops of the soft nanoparticles, the diffusion of center-of-mass can be predicted by a modified Fickian diffusion behavior.

Moreover, it has been emphasized that the particle diameter (D) is a critical parameter in governing the rheological and mechanical properties of nanocomposites [101-103]. Brochard-Wyart and de Gennes proposed a scaling theory [101]. They argued that several polymer characteristic length scales have to be considered regarding particle size effect on the mobilities of chains as well as particles. These critical length scales include polymer random coil size (2 radii of gyration), entanglement mesh size (d_t,), and correlation length (ξ). Cai et al. refined the Brochard-de Gennes scaling theory by considering both the segmental motion and reptation dynamics [102]. According to the refined scaling theory, the motion of a small particle (D < ξ) is not affected by the surrounding segment. The particle motion begins to couple with the segmental motion of the surrounding polymer chains as the particle size becomes bigger ($\xi < D < d_t$). For large nanoparticles (D > d_t), the diffusion of nanoparticles is strongly constrained by the entanglements of the polymeric matrix. To our best knowledge, the previous studies about all-polymer nanocomposites only focused on the particle size in the length scales from the small particle (D < ξ) to intermediate particle sizes ($\xi < D < d_t$). However, few have investigated the role of soft fillers much larger than the d_t with regards to the rheological behaviors of polymeric systems containing soft particles.

In this study, a masterbatch PP with 27 wt.% of micron-sized gelled particle was prepared through a reactive extrusion process, followed by diluting the masterbatch with a proportional amount of linear PP of similar molecular weights. The effects of a soft and deformable gelled particle on PP linear viscoelasticity and strain-hardening behavior were systematically studied. The physical mechanisms responsible for the changes in flow

51

behaviors of gel-containing PPs are proposed. Our findings suggest that the strongly constrained matrix chains near the gelled particles and the matrix chain bridging among the adjacent gel particles both contribute to an increase in the elasticity of PP. The implication of the present study for the preparation of high melt strength polymers is discussed.

4.2 Materials and Methods

4.2.1 Materials

The PP resin, provided by Formosa Plastics Corporation – Taiwan, is a blend of two commercial PP resins of YUNGSOX® PP 1005 and YUNGSOX® PP 1600D at a weight ratio of 3/1 with the same density of 0.90 g/cm^3. The melt flow indexs for YUNGSOX® PP 1005 and YUNGSOX® PP 1600D are 0.5 and 60.0 g/10 min (230 °C), respectively. Dicumyl peroxide (DCP) was purchased from Nouryon. Divinylbenzene (DVB) was obtained from Dow Chemical. Both DCP and DVB were used as received.

The PP containing 27 wt.% of the gelled particle (G27) was prepared in a twin-screw extruder. The temperature setting of the twin extruder machine was set to 180 °C for the first feeder, 210 °C for the second feeder, and 240 °C for the third feeder and die. The rotational speed was 350 rpm. The contents of DCP and DVB were 0.26 wt% and 0.38 wt%, respectively, which were pre-blended with linear resins before being added into the first feeder of the twin-screw extruder. The model gel-containing PPs with a proportional amount of gel content were prepared in a System 40 Haake mixer at 200 °C for 5 min with a rotational speed of 20 rpm. A different weight fraction of G27 (0, 10, 20,

40, 60, 80, 100 wt.%) was melt blended with a linear PP (LPP, YUNGSOX® PP 1120) of a similar weight-average molecular weight (M_w) and molecular weight distribution (MWD) as the G27.

Table 8. Molecular weight and gel content information of LPP and G27.

	M_w (g/mol)	MWD	Gel content,$_{GPC}$ (wt%)	Gel content, $_{extraction}$ (wt%)
G27	2.0×10^5	4.9	27	28
LPP	2.5×10^5	5.1	0	0

4.2.2 Characterization

The molecular characteristics of G27 and LPP were determined by a high-temperature gel permeation chromatography (GPC, Polymer Char GPC-IR®) equipped with an infrared (IR) detector (IR5 MCT) and a viscometer. GPC measurements were made based on a set of narrow MWD polystyrene standards (Polymer Char Narrow PS standards) for calibration. The measurements were carried out at 145 °C with an eluent of 1, 2, 4-triclorobenzene with a flow rate set to 1.0 ml/min. The 200 μL sample solution with a concentration of 1 mg/mL was filtered with a stainless-steel filtration system (Agilent) before being injected into the GPC system to be measured, and the mass recovery after the measurement was recorded.

The gel content was determined by extraction through a Soxhlet apparatus in boiling xylene for 24 h under nitrogen protection. LPP and G27 pallets were placed in a cone-shaped container made of a super-small-particle filtering wire cloth (McMaster-Carr, 316 stainless steel, mesh size 325 × 2,300). The remaining gel was dried in a vacuum oven and weighted. A 3 nm thin platinum layer was coated on the samples using a sputter coater

(Cressington 208HR) before SEM observation. The cryo-fractured surface of G27 and morphology of the gelled particles was then examined by a field-emission scanning electron microscope (FE-SEM) (JEOL JSM-7500F).

Small amplitude oscillatory shear (SAOS) was performed in a strain-controlled rotational rheometer ARES-G2 (TA instruments) using a 25 mm parallel plate geometry under a nitrogen atmosphere. The testing specimen was hot-pressed at 190 °C for 15 minutes into a 100 mm × 100 mm × 2 mm plate, then cut into pieces of 20 mm × 20 mm × 2 mm for rheological measurements. The linear viscoelastic region (LVR) was determined by a strain sweep. A time sweep under a constant strain of 1% at a frequency of 1 rad/s under nitrogen was used to check for possible thermal degradation or structural change during the experiments. Changes in storage modulus (G') and loss modulus (G'') below 5% are considered thermally stable in rheological measurements, and all samples were thermally stable for at least 2 hours, more than the required time for all rheological characterizations. The test frequency range was chosen to be 0.01–100 rad/s, and the sample gap was set at 1.0 mm. A strain of 5% within LVR was used. Extensional viscosity flow measurements were performed using ARES-G2 with an extensional viscosity geometry at 175 °C. To avoid short- and long-range ordered crystalline structure remaining at 175 °C, the loaded sample was first heated to 190 °C for 5 minutes and then cooled down to 175 °C for 10 minutes before the subsequent test.

4.3 Results

4.3.1 Gel Reaction Mechanism

The mechanism of peroxide-initiated crosslinking assisted by a co-agent has been investigated previously; the brief reaction mechanism pertaining to the present study is discussed below [104]. First, DCP was decomposed into alkoxy or methyl radicals at an elevated temperature. Subsequent extraction of the hydrogen atoms on PP backbones resulted in the formation of PP macroradicals. Termination of two macroradicals forms a branched or crosslinked structure. In addition to these grafting and crosslinking reactions, it is well known that radicals preferentially extract the tertiary hydrogen on the PP backbone, forming an unstable tertiary PP macroradical, which easily degrades through β-scission into small fragments. An addition of a co-agent with at least two double bonds can readily react with a tertiary PP macroradical and turn it into a more stable, secondary macroradical. The secondary macroradical is more stable for bimolecular recombination than chains scission, improving the grafting and crosslinking efficiency. The continuous branching and crosslinking reactions eventually form a macro crosslinked gel structure in PP. It is understood that during the crosslinking process, DVB may self-propagate and form a DVB segment as a part of PP branches or crosslinked strands, resulting in a copolymer of poly(propylene-co-DVB) [105]. With the incorporation of only 0.38 wt.% DVB in the process, the main chemical composition of a gelled particle is still considered similar to PP.

4.3.2 Gel Morphology and Branching Degree in G27

MWD curves of G27 and LPP after undergoing a stainless-steel filtration system are illustrated in Figure 16. It is worth noting that the obtained GPC curves represent the results of the post-filtered LPP and G27, meaning only soluble molecules were measured and presented. LPP and G27 exhibit similar values of M_w and MWD. The similar M_w and MWD between these two PP resins ensure that molecular weight (M) and MWD will not be a factor in influencing the investigation of the rheological characteristics of gel-containing PPs.

The intrinsic viscosity [η] curve of LPP follows the Mark-Houwink equation ([η]=kM^a) with a = 0.66 and k = $5.25×10^{-4}$, which conforms with previously reported results [106, 107]. On the other hand, the [η] of the post-filtered G27 deviates from the LPP curve starting from where M is higher than $5×10^5$ g/mol. The reduction of [η] in the filtered G27 is due to the presence of branching, resulting in a smaller molecular size compared to that of its linear counterpart with the same M. Interestingly, it has been reported that there is a critical M of $5×10^5$ g/mol for effective branching and grafting reactions in PP, perhaps due to a higher probability of being attacked for PP chains having higher M [106].

The number of branching points (**B**) can be estimated by the Zimm-Stockmayer equation with an assumption of the random branching distribution [73]:

$$\mathbf{g}' = \left(\frac{[\eta]_{\text{branch}}}{[\eta]_{\text{branch}}}\right)^{\frac{1}{\epsilon}} = \left[\left(1 + \frac{\mathbf{B}}{7}\right)^{0.5} + \frac{4\mathbf{B}}{9\pi}\right]^{-0.5} \quad (10)$$

where **g'** is the chain contraction factor, and ϵ is a draining factor, which is assumed to be 0.5 for a non-free drain star-like polymer [108]. The branching number of G27 ranges from approaching zero branch/backbone at 5×10^5 g/mol to 29 branches/backbone at 2.5×10^6 g/mol. The morphology of the gel obtained by Soxhlet extraction was examined with a SEM, as shown in Figure 17a-b. The gelled particles are well-dispersed in PP when viewed from the fracture surface of G27 (Figure 17c). The gelled particles mostly exhibit a spherical shape. The particle size of the gelled particles ranges between $0.5 - 1.5$ μm. It should be noted that during the filtration process, the gelled particles were densely packed from the original well-dispersed state, yielding a strong particle-to-particle connectivity. During the branching/crosslinking process, the outer region of the gel particles may consist of dangling chains and crosslinked loops (Figure 18). The thin strings connecting amongst the gel particles might be formed due to the presence of dangling chains grafted onto the surface of the gelled particle, or the trapped matrix PP chains from the surface loops.
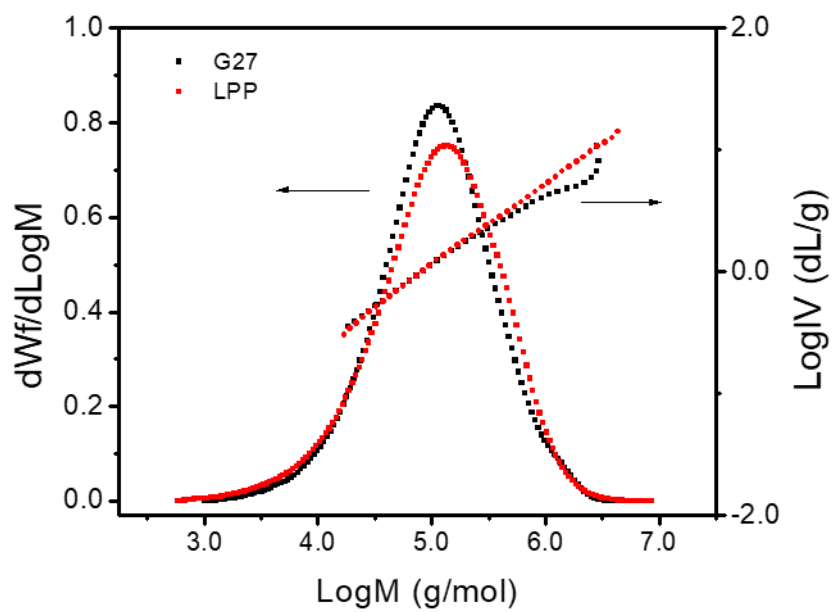
Figure 16. Molecular weight distribution and intrinsic viscosity curves of LPP and G27. (M: molecular weight; W_f: weight fraction; IV: intrinsic viscosity)
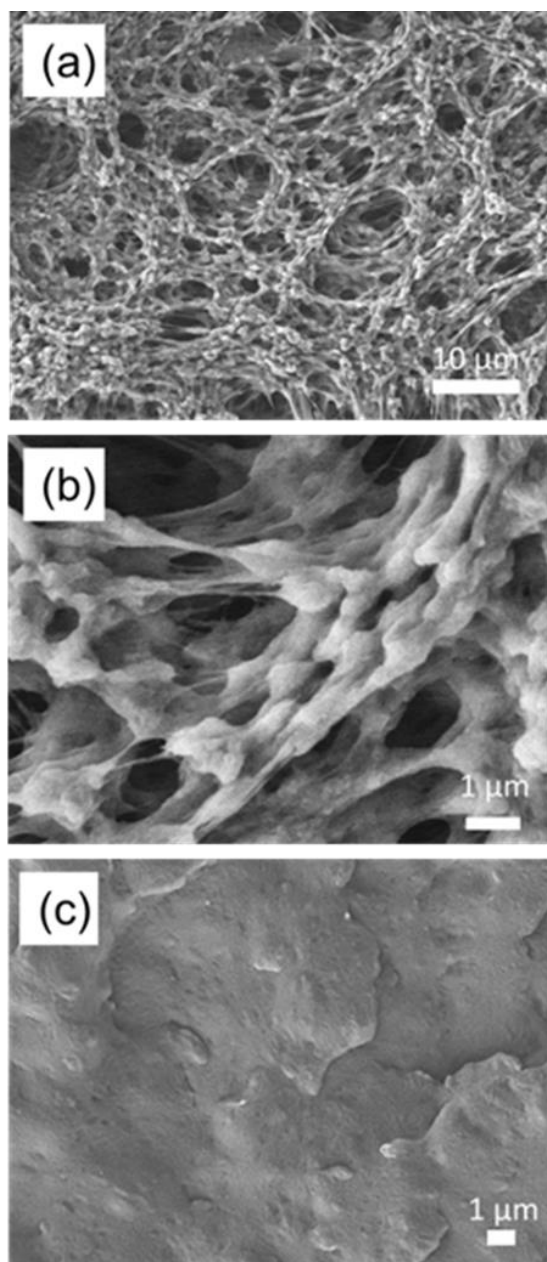
Figure 17. The collected gelled particles after filtration using hot xylene with a 5-micron stainless steel wire cloth at (a) lower magnification, (b) higher magnification, and (c) the cryo-fractured surface of G27
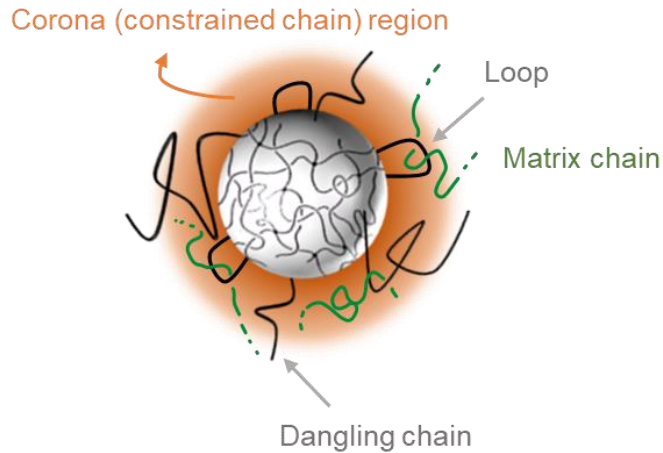
Figure 18. Illustration of the microstructure of a crosslinked PP gel particle with dangling chains and chain loops on the surface.

4.3.3 Linear Viscoelastic Properties

The thermal stability of the PP systems was confirmed using a time sweep under a small, constant strain of 1% at a frequency of 1 rad/s, as shown in Figure 19. For clarity, only the results of LPP and G27 were plotted. The changes of G' and G'' were less than 5%, suggesting no additional, discernable reactions, such as grafting, crosslinking, or degradation, happening within a 2-hour experimental time frame. The G', G'', and complex viscosity (η^*) obtained from the small amplitude oscillatory shear measurements for the LPP and gel-containing systems are shown in Figure 20. G', G'', and η^* exhibit a strong frequency dependency in all the gel-containing PP systems. The linear viscoelastic properties at high frequencies are dominated by the polymer matrix and its entanglement density [109, 110]. At high frequencies, there are no distinct differences among the samples. As the frequency decreases, the contribution of gelled particles on rheological behavior becomes more significant, and the G', G'', and η^* increase with an increase in

gel content. The more substantial enhancements in G', G'' and η* at lower frequencies are attributed to the longer response time of polymer chains interacting with the gel particles, further restricting molecular motions [109, 110]. The filler contribution to polymer linear viscoelasticity varying at different frequencies has been reported in several polymeric systems, such as poly(ε-caprolactone)/multi-walled carbon nanotube [111], poly(lactic acid)/fine fiber made of poly(butylene terephthalate) [112], and poly(methyl methacrylate)/graphene nanocomposites [23].
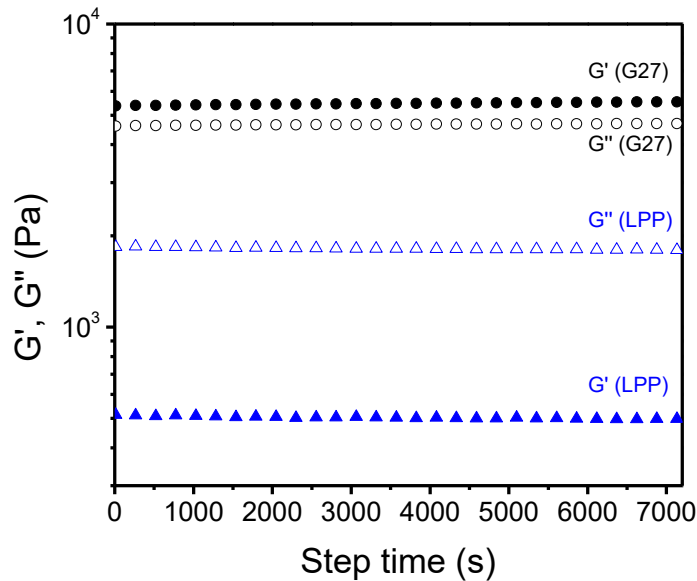
Figure 19. Storage modulus (G') and loss modulus (G'') as a function of time at a strain of 1% at a testing frequency of 1 rad/s for 7200 s at 190 °C under nitrogen.

After a stress/strain was applied at a given frequency in a dynamic oscillatory shear test, the values of G' represent the capability of storing energy, and G'' demonstrates its energy dissipation capability. The scaling factor β of G' (G'~ ω^β) in the terminal region was obtained from the logG'-logω plot. The β of LPP is 1.8 in the low-frequency region,

similar to the typical low-frequency terminal behavior of linear chains, i.e., $G' \sim \omega^2$. The values of β being less than the typical value of 2.0 might be due to the broad MWD of LPP [113]. With 2.5 wt.% gel, G2.5 exhibits almost the same G'' value as LPP, but with a slightly higher G' in the low-frequency regions. The findings suggest that the 2.5 wt.% gel contributes to the increase in elasticity while having negligible contributions to PP energy dissipation. By incorporating higher gel content, both G' and G'' gradually increase and become less frequency-dependent. The values of β decrease from 1.8 for LPP to 0.4 for G27, suggesting that a longer molecular relaxation process is involved upon gel incorporation. The longer relaxation process may arise from gel-polymer and gel-gel interactions. Moreover, G27 exhibits a gel-like behavior, whose G' is higher than G'' within the whole testing frequency range (Figure 20c).

Figure 20d shows η^* versus frequency. LPP exhibits a frequency-independent viscosity at low frequencies, i.e., Newtonian plateau, followed by shear-thinning behavior as the frequency increases. Similar to G' and G'', the values of η^* increase with gel content. In addition, the Newtonian plateau region gradually decreases with more gel content, and eventually disappears. PPs containing over 16 wt.% of gelled particles exhibit a remarkable shear-thinning behavior. Since the measurements were carried out in the linear viscoelastic region with no time dependence observed during the time sweep, it is reasonable to assume that there were no structural changes within the experimental time frames, i.e., change in gel distribution, degradation, crosslinking reactions, etc. The increase in η^* with gel content is attributed to the frictional phenomena among the polymer

chains and gelled particles. These frictional phenomena lead to a higher resistance to flow, thereby increasing η* with increasing gel content [114].
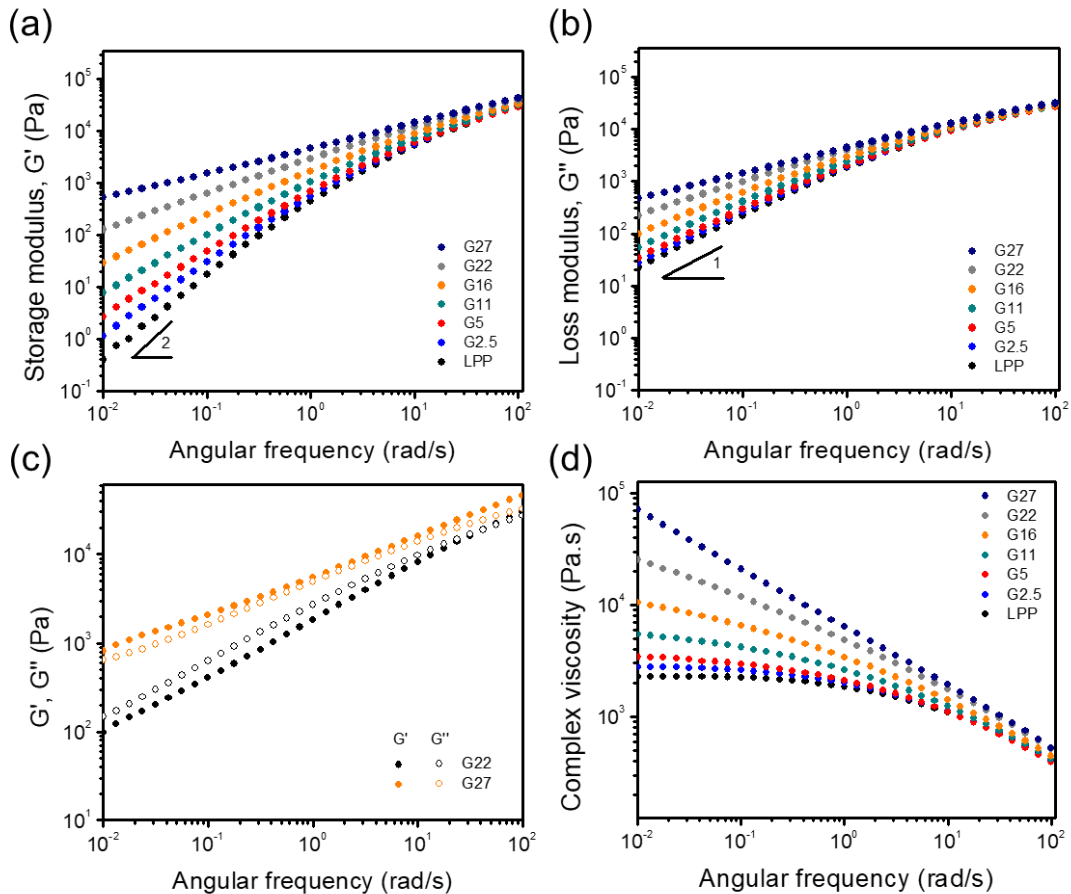
Figure 20. (a) G' as a function of angular frequency for LPP and all gel-containing PP systems, (b) G'' as a function of angular frequency for LPP and all gel-containing PP systems, (c) Frequency dependence of G' and G'' values for G22 and G27, and (d) η* of LPP and gel-containing PP systems as a function of angular frequency

4.3.4 Uniaxial Elongational Flow Behaviors

Branching and filler incorporation have been used to increase the polymer melt strength to prevent the molten polymer from sagging and cell coalescence [93, 115, 116]. Trouton found that the elongational viscosity always equals three times the viscosity in shear flow for a Newtonian fluid [117]. This finding has been validated in most polymer-based systems. Strain hardening means that the elongational viscosity deviates from a linear viscoelastic baseline curve estimated by the Trouton ratio. That is, the elongational viscosity at a given strain rate is increased significantly under a large strain. Figure 21 shows the transient extensional viscosity of the selected gel-containing PP systems as well as the reference line predicted by the Trouton ratio. All the gel-containing PPs show significant strain-hardening at all strain rates under a large strain condition. The degree of strain-hardening can be quantified by the time-dependent strain-hardening coefficient χ $(t, \dot{\varepsilon})$, which is defined as,

$$\chi(t, \dot{\varepsilon}) = \frac{\eta_e^+(t, \dot{\varepsilon})}{3\eta_s(t)} \tag{11}$$

where η_e^+ is the transient uniaxial elongational viscosity, η_s is the transient shear viscosity, t is the time, and $\dot{\varepsilon}$ is the strain rate. The values of χ $(t, \dot{\varepsilon})$ are plotted as a function of Hencky strain (ε_H), which is obtained by an equation of $\varepsilon_H = \dot{\varepsilon} \times t$. LPP exhibits no strain-hardening at all testing strain rates, and its value of χ is close to unity. The χ increases with the incorporation of gelled particles, even at a low gelled particles loading. The increase in the degree of strain-hardening is likely attributed to the strong resistance

of the elongational flow resulting from the constrained chains near the gel particles, elongated gel particles, and gel-gel interconnection bridged by PP matrix chains.
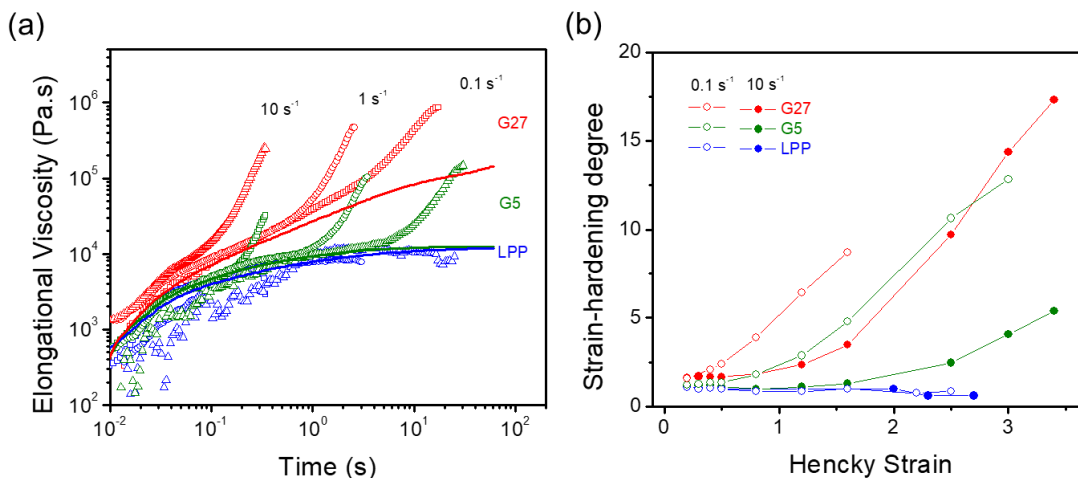
Figure 21. (a) Uniaxail elongational viscosity at three different strain rates of 0.1, 1, and 10 s^{-1}. The solid line presents the threefold of the transient viscosity as measured at a shear rate of 0.1 s^{-1} (b) The strain hardening degree as a function of Hencky strain at strain rates of 0.1 and 10 s^{-1}.

4.4 Discussion

Rheological behaviors of PPs containing an increasing amount of gelled particles have been investigated systematically using SAOS and elongational flow measurements. The gelled particle in the present study exhibits a spherical shape with dangling chains grafted onto the particle's surface. Dissimilar to rigid and impenetrable carbonous and metallic fillers, the gelled particle in this study is deformable and has the same chemical composition as the PP matrix. Based on the above observation and those of soft particles investigated by others [97, 99], the gelled PP particle morphology in a PP melt is proposed and illustrated in Figure 18. The proposed gelled PP particle exhibits a core-corona

structure composed of a crosslinked core and an outer corona region where the chain loops and dangling chains strongly interact with the surrounding PP matrix chains. The corona region, also called the immobilized layer, has been observed by direct experimental observation and considered in theoretical models [118-121]. The presence of the corona region has been shown to be responsible for a sol-gel transition and mechanical reinforcement.

In the present study, the radius of gyration of the PP random coil with M_w of 2×10^5 g/mol is around 15 nm. In addition, the entanglement mesh size (d_t,) of the PP is obtained through the equation of $d_t = bN_e^{\frac{1}{2}}$, where b is PP statistical length, i.e., Kuhn length, and N_e is the number of Kuhn monomers in an entanglement strand. The entanglement mesh size of PP is around 6.7 nm, close to the previously reported value [122]. Therefore, the micron-size gelled particle is undoubtedly well above the entanglement mesh size. The entanglements strongly restrict the motion of the gelled particles. The gelled particles larger than d_t generally move via the dynamical constraint release after the relaxation of entanglements [103]. The terminal relaxation time (τ_{te}) is the time required for a molecule chain to complete a configurational rearrangement after snaking out of the tube constructed by entanglements [123, 124]. τ_{te} can be estimated by the reverse of the crossover frequency of G' and G''. The values of τ_{te} for all the gel-containing PP systems are listed in Table 9 [123, 124]. It has been demonstrated in Section 3.3 that the increase of G', G'', η^* is due to a more significant contribution by gelled particles at lower frequencies. The stronger reinforcement happens particularly in frequency regions lower than the neat PP entanglement relaxation time (τ_e) of 0.76 s (85.2 rad/s). The required time

for PP chains to rearrange increases with gel incorporation and becomes infinite if gel content is more than 27 wt.%. The results suggest that the dangling chains as well as the threaded PP matrix chains into the surface loops form dense entanglements with PP matrix. Increase in entanglement density increases the resistance for chain relaxation, and thus, the τ_{te} of gel-containing PPs.

Batchelor extended Einstein's theory and proposed a simple correlation of viscosity to an impenetrable particle volume fraction in a dilute solution, which is $\frac{\eta}{\eta_{matrix}} = 1 + 2.5\phi + 5.9\phi^2$, where φ is the volume fraction of filler [125]. As shown in Figure 22, η^* at a frequency of 0.01 rad/s and zero-shear rate viscosity (η_0) determined by fitting the complex viscosity data with the empirical Cross equation, $\eta^* = \frac{\eta_0}{1+(k\omega)^m}$, where k is a constant, and m is the shear-thinning index [126, 127]. The Einstein-Batchelor prediction fits reasonably well below η^* at 0.01 rad/s and η_0 at a low gel volume fraction. The Einstein-Batchelor equation underestimates the actual gel particle volume fraction effect, most likely due to the fact that the corona region of the gel particle was not considered as a part of the gel particle. The effective volume of a gelled particle influencing the PP flow properties should be much larger than the volume fraction converted directly from the weight fraction of the soft gelled particle, which accounts for only the crosslinked core. The effective volume felt by the PP matrix can be obtained via the Einstein-Batchelor equation. As shown in Table 9, the effective volume fraction for G2.5 is 8 vol.%, and the ratio of the effective particle radius (R) to the core radius (r) is 1.47. This diameter ratio remains at 1.47 up to 11 vol.% gel, where the effective volume fraction is 36 vol.%. Once over the 16 wt.% gel, the significant divergence of this ratio is

observed, possibly due to the strong gel-gel interaction, which renders it invalid from the assumption of the Einstein-Batchelor model that there is no particle-particle interaction expected in the suspension.
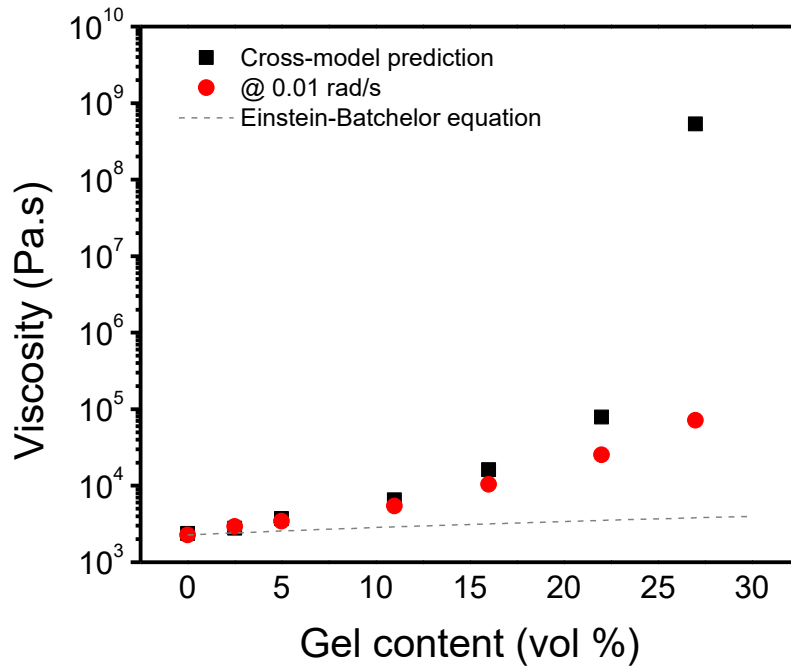
Figure 22. The complex viscosity measured at 0.01 rad/s and the zero-shear viscosity estimate by the Cross model are plotted as a function of gel content. The volume fraction and weight fraction are the same since the density of the gelled particle and the PP matrix are assumed to be the same. The dash-line is predicted by the Einstein-Batchelor equation.

Table 9. The relaxation time for the complete chain reconfiguration, the ratios of effective particle radius to core radius, and the effective volume fraction for all gel-containing PP systems.

	τ_{te} (s)	R/r	Effective volume fraction by Einstein-Batchelor prediction
LPP	0.74	n/a	n/a
G2.5	0.80	1.47	0.08
G5	0.94	1.47	0.16
G11	1.23	1.47	0.36
G16	2.03	1.61	0.68
G22	4.48	n/a	n/a
G27	∞	n/a	n.a

It has been reported that the percolation threshold of rheological behaviors is the point where the interparticle distance is shorter than the two radii of gyration (random coil size) [128, 129]. The interparticle distance (IPD) for a random, well-dispersed particle is estimated by IPD = $D[(\phi^*/\phi)^{1/3}-1]$, where D is the diameter of the particle, ϕ^* is the maximum packing volume fraction of 0.63 [130]. The critical IPD as a function of the particle size is plotted in Figure 23. The required volume fraction for achieving the percolation threshold is low for nanoparticles, which has been reported previously [131, 132]. With a micrometer size particle-like in the present PP gel systems, the critical percolation threshold volume reaches a plateau and increases slowly with particle size. At 16 wt.% gel incorporation, assuming the constrained corona thickness is the same as in G2.5, G5, and G11, the effective volume fraction of G16 is equal to 51 vol%, which is close to the obtained percolation volume fraction. Therefore, partial chain bridging between the gelled particles results in additional resistance for the flow, which accounts for the failure of the Einstein-Batchelor prediction. As the IPD becomes smaller than the coil size $\approx$ 30 nm, the molecular chains located in between the gel particles will be

69

significantly constrained by the gelled particles. Several previous studies have observed

the occurrence of the extension of molecules, bridged by the adjacent particles, and the

formation of a polymer-bridged 3-D gelled network over the percolation threshold

concentration [129, 133, 134], which explains the significant increases in τ_{te} of PP having

over 16 wt.% gel.
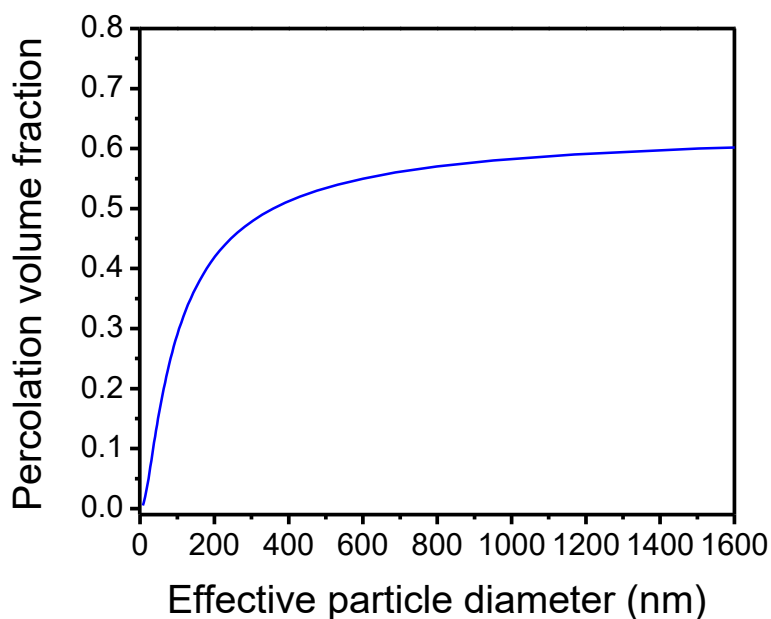
Figure 23. Percolation volume fraction as a function of effective particle size.

In the present study, we have introduced PP soft gelled particles to modify the

rheological behavior of PP. The gel particle size is well above the entanglement mesh size,

and its flow is strongly constrained by entanglements. To the best of our knowledge, the

present study is the first to investigate the dynamics of soft particles much larger than d_t

in a polymer melt. Considering the corona region formed by the dangling chains and

strongly constrained matrix chains near the particle surface, the effective volume fraction of the core-corona structure explains the significant increase in G', G'', η* and strain-hardening level. The formation of the corona region is attributed to the constrained chain retarded by surface loops and entangled dangling chains. With the incorporation of PP gel particles, the PP processibility can be significantly improved.

4.5 Conclusion

The rheological behaviors of gelled particle-containing PP composites have been investigated with small amplitude oscillatory shear and extensional flow measurements. In the small amplitude oscillatory shear measurements, G', G'', and η* values rise with an increase in gelled particle incorporation, especially at low frequencies. The dynamics of these gel-containing systems are strongly influenced by the constrained chains near the gel surfaces and the ability of polymer chains to bridge surrounding gels, depending on the surface-t-to-surface interparticle distance. The extensional flow viscosity indicates that the gelled particles with a corona consisting of chain loops and dangling chains can serve as star-like particles, increasing entanglement density and enhancing the strain-hardening at low gelled particle loadings. The present study demonstrates an alternative method to improve the strain-hardening degree in PP without a significant change in density profile and requirements for additional fillers. The present study shows the chain and particle dynamics in an all-polymer composite with a particle size much larger than the entanglement mesh size.

CHAPTER V

EFFECT OF LONG-CHAIN BRANCHING MOLAR FRACTION ON SCRATCH

BEHAVIOR OF POLYPROPYLENE[*]

Polymers containing a certain amount of LCB structure are expected to possess improved mechanical properties over those of the linear structure counterpart. However, fundamental knowledge on the structure-property relationship in LCB containing PP is still elusive. In this chapter, a set of model LCB-PP systems containing an increasing molar fraction of LCB (5-19 mol %) were used to determine how LCB content may influence the scratch behavior of PP. It is shown that only 5 mol % of LCB content in PP is required to improve resistance against scratch-induced fish-scale formation by over 25%. The improvement of scratch resistance is attributed to the increases in entanglement density in LCB-containing PPs, which is evidenced by their creep-recovery behavior. The present study demonstrates that incorporating LCB in PP leads to higher viscoelastic recovery and increased tensile strength, which account for the observed improvement in scratch performance.

5.1 Introduction

To better control the processing conditions and the product properties, extensive works have focused on characterizing the level and extent of LCB using triple-detector gel permeation chromatography, nuclear magnetic resonance, and rheology [55, 57, 62, 63]. However, only a few studies have investigated the effect of LCB on the mechanical properties of polymers. Li et al. investigated how the LCB influences the mechanical properties of recycled PPs prepared by reactive extrusion. It is found that the tensile strength increases with LCB incorporation due to a higher entanglement density and its stronger intermolecular interaction, preventing the chain slippage during the uniaxial tensile test [135]. Wang et al. studied the LCB poly(butylene succinate) synthesized by esterification and polycondensation and its mechanical properties [136]. They found that the tensile strength was improved by 31%, while the elongational at break remained at a low LCB content and then decreased with further LCB incorporation. Zhao et al. probed the tensile and notch impact strengths of LCBPPs synthesized by melting grafting reaction with peroxide and polyfunctional monomer [137]. They believed that the increases in the tensile strength and impact strength of LCBPPs were mainly due to the additional energy contribution from the disentanglement or breakage of LCB chains.

The scratch performance of polymers has recently been recognized as one of the required engineering properties because of their importance in automobile, household, and optical applications. Unlike ceramics and metals, the vulnerability of polymeric materials to surface deformation and damage has been a major concern to product designers, manufacturers, and consumers. Scratch is one of the most common types of surface

damage and can severely impact the aesthetics and functionalities of a product. With the establishment of the standardized ASTM/ISO scratch test method, which is a linearly increasing normal load scratch test, numerous experimental and simulation efforts have been pursued to gain fundamental knowledge on polymer scratch behaviors [138-144]. There has been a great interest in learning about how the entanglement density and intramolecular interaction can influence the mechanical and scratch behaviors of polymers [145-149]. Moghbelli et al. carried out a study on two model PPs with two weight-average molecular weights (M_w) of 416,000 and 305,000 g/mol to understand how the molecular weight (MW) of PP influences scratch resistance [148]. It is found that the scratch resistance of PP is improved with higher MW. The authors claim that the higher entanglement density and better elastic recovery of high MW PP contribute to its better scratch performance. More recently, Xiao et al. examined three model thermoplastic polyurethane (TPU) elastomers with different MW but with the same hard and soft segments ratio. Their study also shows that the onset of cracking and material removal is delayed as the MW of TPU is increased because of their corresponding tensile strength enhancement [146]. Additionally, Browning et al. studied a set of styrene-acrylonitrile (SAN) random copolymers with variations in MW and acrylonitrile (AN) content. They indicate that an increase in both MW and AN content improves the tensile strength and, thereby, the scratch resistance of SAN due to their higher entanglement density and stronger inter-chain interactions [149].

The above findings suggest that a stronger molecular interaction and higher entanglement density may improve the tensile strength of a polymer, thereby delaying the

onset of scratch damage formation. However, little has been done to examine the effect of LCB molar fraction on scratch properties. With an increasing demand for high melt strength PP in engineering applications, it is necessary to investigate how the LCB content influences the scratch behavior of PP. Based on a recently established quantitative method to determine LCB molar fraction in PP by using a combination of GPC and rheology characterizations, the LCB molar fraction in a polymer can now be reliably quantified [150]. Consequently, it becomes possible to learn how the mechanical properties and scratch behavior can be manipulated by changing the LCB molar fraction. The present study focuses on understanding how the LCB molar fraction influences the scratch behavior of LCBPP and their tensile properties. The usefulness of the present study for the development of scratch-resistant polymers is also discussed.

5.2 Materials and Methods

5.2.1 Materials

The pallet-form of LCBPP model systems modified with increasing amounts of a proprietary coupling agent which introduce LCB in PP were supplied by Braskem, USA [71]. A recently published paper has described the detailed branching reaction, coupling agent, and sample preparation method [150]. The composition of the model systems and the LCB molar fraction in each sample was determined by a combination of GPC and rheological approaches and summarized in Table 10 [150]. Scratch specimens were prepared using a hydraulic press at a pressure of 200 psi at 175 °C for 25 minutes. The compression-molded scratch specimens were slowly cooled to room temperature and

annealed at 60 °C overnight before testing. The dimensions of each specimen are 10 mm × 10 mm × 3 mm.

Table 10. Formulation of the model PP system.

Samples	Antioxidant (wt %)	Coupling agent (wt %)	LCB molar fraction[150] (%)
PP		0	0.0
LCBPP-5	0.1	2	5.1
LCBPP-13		5	13.4
LCBPP-19		8	19.1

5.2.2 Characterization

Thermogravimetric Analysis

Thermogravimetric analysis (TGA) was conducted with a Q500 thermogravimetric analyzer (TA Instrument). The temperature was first ramped from room temperature to 175 °C at a ramped rate of 10 °C/min, and then the samples were conditioned at 175 °C under an air environment for 50 minutes.

Creep-recovery Measurement

An ARES-G2 strain-controlled rheometer (TA Instruments) with a 25 mm parallel plate geometry was used to measure creep-recovery under a nitrogen atmosphere at 190 °C. A two-hour time sweep was performed at a frequency of 1 Hz at 190 °C to check thermal stability, and all samples were considered thermally stable with fewer than 5% changes in storage modulus and loss modulus. Creep-recovery measurements were done at 190 °C, and a stress of 10 Pa was applied instantaneously and held for 300 s, followed

by removing the stress and kept for 300 s. The changes in strain were recorded. A stress control step was performed before each creep-recovery measurement.

Surface Crystallinity

Surface crystallinities of the tested specimens were measured using differential scanning calorimetry (DSC) (Q20, TA Instruments) under a nitrogen gas flow rate of 40 mL/min and a heating rate of 10 °C/min. About 5 mg surface layer (< 150 μm) was carefully removed and collected from the specimen using a fresh razor blade to examine the surface crystallinity. The crystallinity of each sample was determined based on its heat of fusion from the first scan DSC against the heat of fusion of the 100% crystalline PP (207 J/g) [151].

Wide Angle X-ray Diffraction

Wide-angle X-ray diffraction analysis (WAXD) was performed on the surface of the tested specimens by a Bruker-AXS D8 Advanced Bragg-Brentano X-ray Powder Diffractometer. Diffraction patterns were collected at room temperature for 2 θ from 4° to 30° to measure the crystalline structure near the surface of each model PP with a step size of 0.07°.

Uniaxial tensile true stress-strain curve generation

Uniaxial tensile tests were performed using an RSA-G2 Solids Analyzer (TA Instruments) with a microfilm tensile fixture. PP sheets around 200 μm thick were first

prepared by the hot press at 175 °C. Dumbbell-shaped tensile bars were carefully cut out from the PP sheets using a fresh razor blade, and the cutting edge was polished with 2400 grit number polishing paper to remove surface defects and asperities. Before the test, a black ink permanent marker was utilized to apply random dots on the gauge section of specimens for digital image correlation (DIC) analysis. The tensile specimen was loaded on the RSA-G2 for a tensile test at a crosshead speed of 5 mm/min. The shape changes on the sparkle pattern were recorded using a Canon EOS 5D Mark II DSLR camera and were then analyzed using a VIC-2D^{TM} software package (Correlated Solutions, USA) to capture instantaneous stain in the vertical and lateral directions. The true stress was calculated by dividing the load by the instantaneous cross-sectional area.

Scratch Test

Scratch tests were conducted at room temperature following the standard ASTM D7027-05/ISO 1925:08 method [138, 139]. A linearly increasing normal load across the scratch was applied by the Generation 5 scratch machine manufactured by Surface Machine Systems (College Station, TX) with a 1 mm stainless spherical tip from 1 to 50 N. The scratches were conducted over a distance of 80 mm at two speeds: 10 and 100 mm/s. The coefficient of friction (COF) was determined using the same scratch machine by applying a constant low normal load of 5 N over a distance of 100 mm using a 10 mm × 10 mm flat square stainless tip at a speed of 10 mm/s. At least three tests were carried out for each speed on each sample to obtain both the average and standard deviation values of the critical loads of damage transitions.

Scratch Damage Analysis

Scratch deformation was visualized using a violet laser scanning confocal microscope (VLSCM) (KEYENCE VK-9700K). The height resolution is up to 1 nm, and its violet laser wavelength is 408 nm. Onsets of fish-scale and groove formation were located under 20X magnification using VLSCM, and the corresponding loads were determined using the applied load-vs-distance curves produced by the scratch machine. Scratch topography was imaged under a laser mode with 20X magnification. Tilt correction was applied to prevent the possibility of uneven alignment during the imaging process.

Scratch Visibility Analysis

To examine the scratch visibility, the samples were imaged in a Black Box Imager (Surface Machine Systems, College Station) with a high-resolution camera (Canon EOS REBEL i3 DSLR with Cannon EFS 18-55 mm zoom lenses). The images were then analyzed using the Tribometrics® software package provided by Surface Machine Systems. A contrast of 2% and continuity of 90% were used. To validate the machine vision analysis results, five trained human subjects were also asked to observe the unmarked scratched specimens individually and determine the onset of scratch visibility under the same lighting conditions as in the black box. The corresponding critical loads for scratch visibility were determined.

5.3 Results and Discussion

5.3.1 Thermal Stability

Since the scratch specimens were prepared using a hydraulic hot press at 175 °C in air for 20 min, the thermal stabilities of PP at 175 °C in air were also monitored using TGA (Figure 24). No significant weight change was detected in 25 minutes, suggesting that the samples remained thermally stable during the sample preparation at 175 °C.
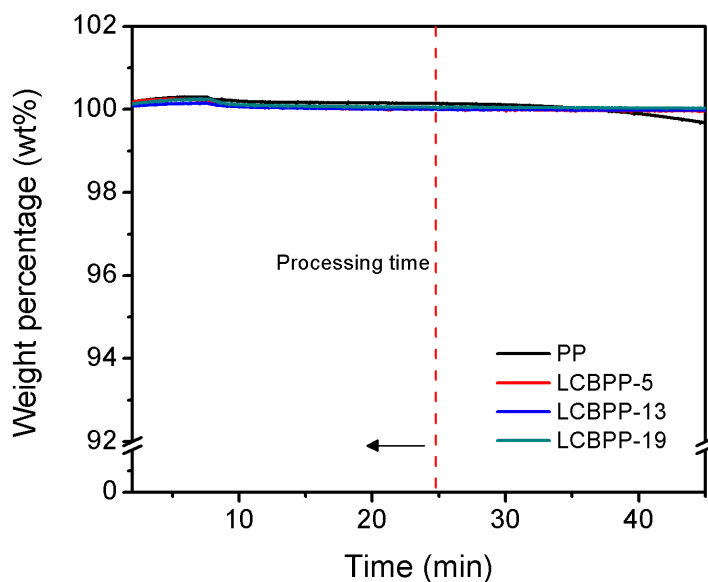
Figure 24. The TGA weight change profile of PP samples in air at 175 °C for 50 minutes.

5.3.2 Creep-Recovery Experiment

To determine the possible entanglement effect of LCB on viscoelastic recovery in PP, a creep-recovery experiment was conducted. A test temperature of 190 °C on PP melt was chosen to maximize the signal-to-noise ratio and observe the differences in creep-recovery strain response within the instrument limit (Figure 25 (a)). Upon applying a

constant stress of 10 Pa at 190 °C, the PP reaches its steady viscous flow (i.e., at constant strain rate) immediately, indicating that linear PP is liquid-like. In contrast, LCBPP-19 with the highest LCB molar fraction shows an instantaneous viscoelastic recovery phenomenon. Moreover, it is noted that incorporating more LCB molar fraction increases not only the resistance to deformation but also the ability to recover from the deformation (Figure 25 (b)). The above result suggests that LCBPPs exhibit higher network integrity, i.e., high entanglement density, to resist deformation and recover some deformation upon release of the applied stress. This is consistent with our previous rheological findings that an increase in LCB molar fraction leads to a higher entanglement density and stronger cohesive strength in PP, thus exhibiting a higher zero-shear viscosity, lower phase angle, and higher storage modulus in the terminal region of small amplitude oscillatory shear measurements [150].
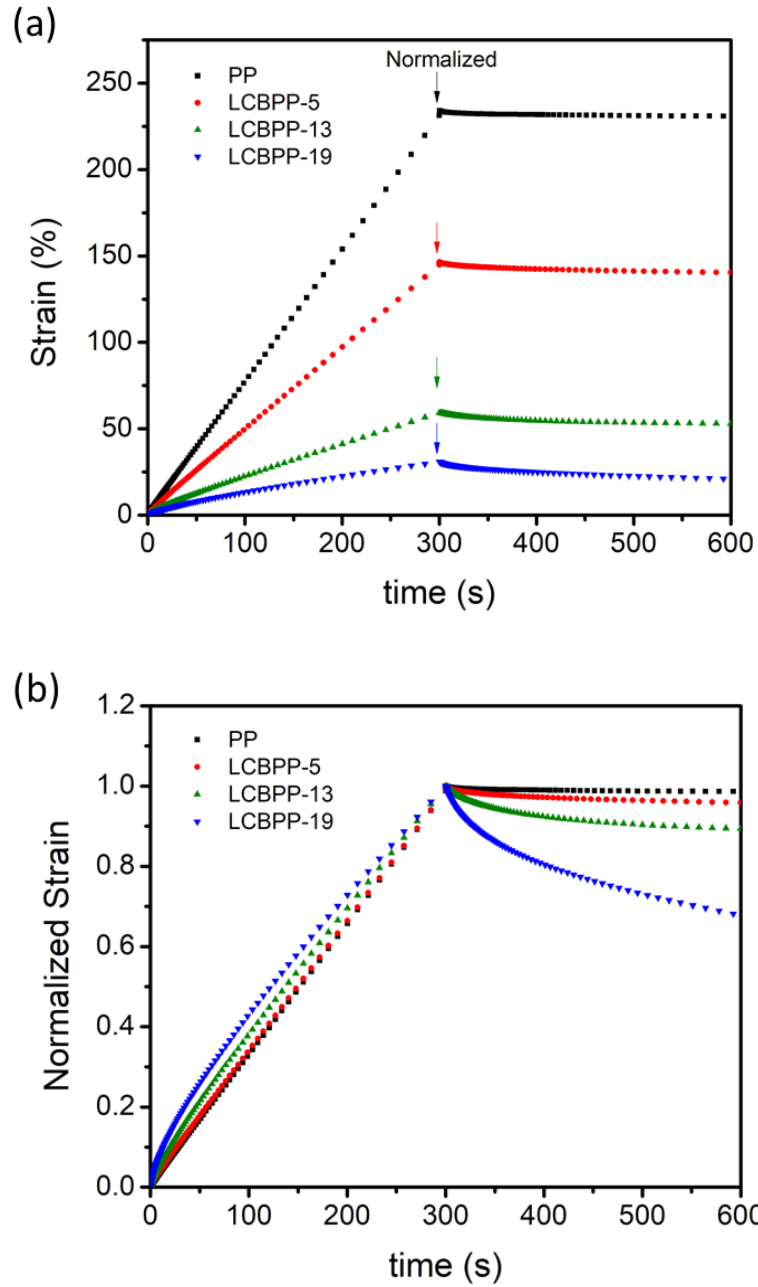
Figure 25. (a) Creep-recovery experiment at 190 °C with applied stress of 10 Pa for 300 s and removal of the applied stress for recovery to take place for another 300 s. (b) Normalized strain as a function of time for the model linear PP and LCBPPs.

5.3.3 Surface Crystallinity and Crystal Structure

The crystalline forms of PP include monoclinic α-form, trigonal β-form, and orthorhombic γ-form crystallites, of which α-form is the most common. β-form and γ-form crystallites may be formed by adding nucleating agents or processing at specific conditions [152-154]. Since it has been demonstrated that crystallinity and surface features can significantly influence the mechanical properties and scratch behavior, it is crucial to examine the surface characteristics of the tested PP and LCBPP specimens to allow for unambiguous determination of the LCB molar fraction effect on the scratch behavior of PP [148, 154, 155].

The crystalline structure on the surface of the model systems was examined by the wide-angle X-ray diffraction (WAXD) patterns, as shown in Figure 26. The angles at 14.5, 16.9, 18.5, 21.2, and 25.5 correspond to diffraction peaks on the (110), (040), (130), (111), and (060) lattice planes of α-form crystal, respectively. The diffraction peak at 21.8 is attributed to both the (−131) and (041) lattice planes of α-form crystal [156, 157]. There is only minor variation in crystal structure among the model PP systems. No evidence of β-form and γ-form crystallites were not found in these samples. The crystallinity near the surface of the model PP systems was further obtained from DSC and listed in Table 11. As shown, the negligible differences in crystallinity and crystal structure among the model systems near the surface indicate that they should not be a factor to influence their scratch behaviors.

It has been uncertain regarding how the LCB structure influences the crystallization behavior of polymers. Some researchers suggest that branching points may

act as nucleation sites to facilitate nucleation and consequently increase crystallinity. Nofar et al. investigated the crystallization kinetics of both linear and LCB polylactide (PLA). They found that LCBPLA has a higher crystallinity compared to linear PLA due to the presence of the branching points, which serve as nucleation sites for achieving a higher crystallinity [158]. Li et al. studied the crystallization behavior of recycled PPs modified with dicumyl peroxide, maleic anhydride monomer, and glycidyl methacrylate [135]. They found that LCB decreases the half-time of crystallization due to increased nucleating sites to facilitate PP crystallization. On the other hand, Wang et al. found that LCB reduced structural regularity, thus decreasing crystallinity in their investigation on the crystallization behavior and crystalline morphology of LCB poly(butylene succinate) [136].

For the model LCBPPs, their branching numbers range from 0.4 to 3.1 branches per molecule, which is considered to be a loosely branched architecture [150]. Additionally, the rheological characterization also suggests that the branch lengths in all the LCBPP systems are significantly longer than the entanglement molecular weight of PP. The long branches in the PP backbone are equally capable of participating in the crystallization process. Consequently, LCB incorporation does not have any noticeable impact on the crystallinity of PPs.
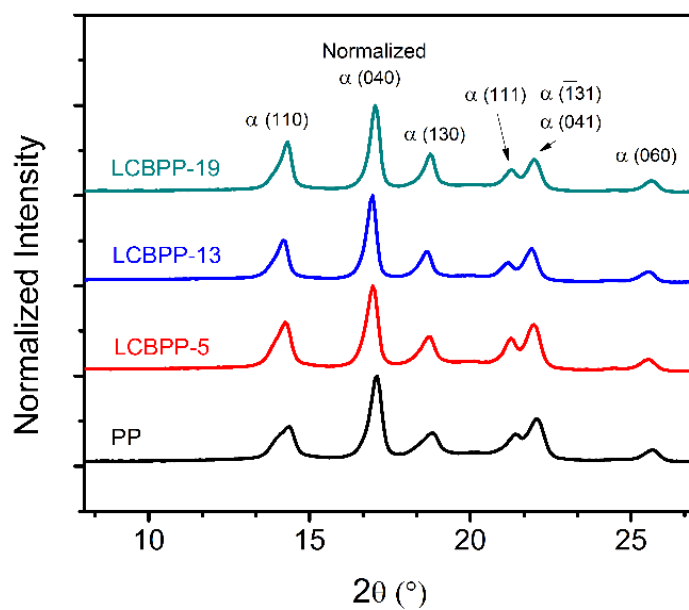
Figure 26. WAXD measurement.

Table 11. Surface crystallinity obtained from DSC.

Name	Surface crystallinity (%)
PP	48.8±0.9
LCBPP-5	49.3±1.0
LCBPP-13	50.5±1.7
LCBPP-19	50.1±1.5

5.3.4 Uniaxial Tensile True Stress-strain Behavior

It has been found in the previous study that tensile and compressive properties are closely related to the scratch behavior of polymers [143, 144, 146]. The true stress-strain curves of the model systems are shown in Figure 27, and their corresponding tensile properties are summarized in Table 12. When compared against the neat PP, all the LCBPP systems exhibit higher tensile strength and higher elongation at break, while the Young's modulus remains the same. Young's modulus is known to be closely related to crystallinity and small strain related local molecular motions, which can be affected by molecular structure, side group type and size, and entropic contribution [159, 160]. An increase in entanglement density by increasing MW of a polymer has been found to improve the tensile strength but not Young's modulus [161]. In LCBPPs, the only difference among the model systems is the presence of up to a few LCB chains per PP molecule. These few LCB chains are unlikely to alter PP resistance against small-strain deformation. Therefore, the Young's modulus exhibits negligible changes among the model systems.

On the other hand, tensile strength and ductility are known to be influenced by the presence of defects, tie-chain density, entanglement density, molecular weights, crystallinity, etc. [147, 161, 162]. Chain entanglements, which serve as physical crosslinks to resist disentanglement, can help stress redistribution among molecules and sustain higher stresses before failure, i.e., a higher tensile strength [147, 149, 163]. However, further increase in entanglement density in LCBPP does not further improve tensile strength and elongation at break, indicating an only marginal benefit of additional

LCB molar fraction in tensile property improvement of PP. This corresponds to the previous findings that after reaching a critical entanglement density, a further increase in molecular weight becomes less effective in improving tensile strength [145, 147].
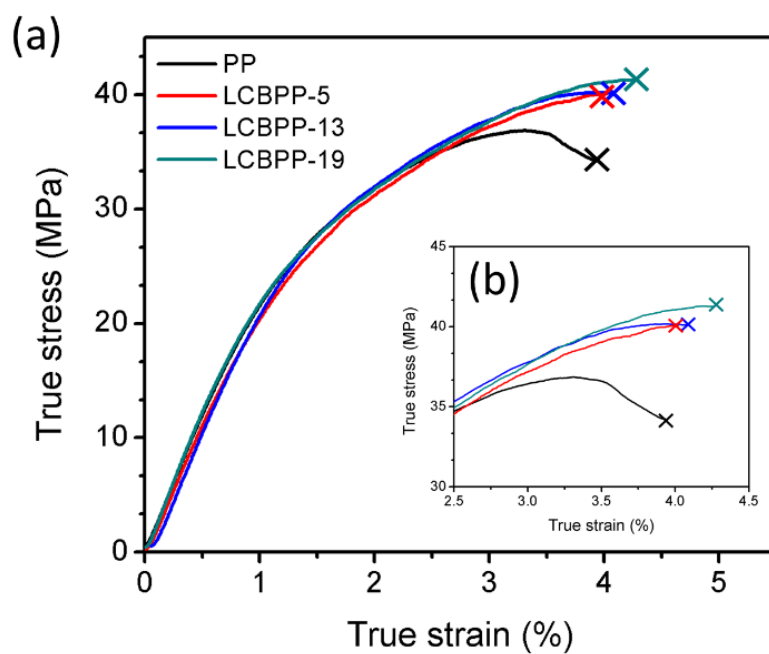
Figure 27. (a) True stress-strain curves of the model linear PP and LCBPP systems. (b) Stress-strain curves in a strain range of 2.5-4.5%.

Table 12. Tensile properties of the model systems with increasing polyfunctional monomer content.

Name	Modulus (GPa)	Tensile strength (MPa)	Elongation at Break (%)
PP	1.63 ± 0.05	36.6 ± 0.5	3.8 ± 0.4
LCBPP-5	1.65 ± 0.07	39.3 ± 0.4	4.7 ± 0.6
LCBPP-13	1.66 ± 0.02	41.5 ± 0.6	4.5 ± 0.8
LCPPP-19	1.64 ± 0.04	42.4 ± 0.7	4.6 ± 0.2

5.3.5 COF and Surface Roughness Measurements

The COF and surface roughness of the four model PP systems are listed in Table 13. The obtained values are similar to each other, indicating the surface features among all the model systems are about the same. Based on the above surface characteristics and similar surface crystallinities, it can be concluded that the differences in scratch behavior among the model PP samples, if any, should be due to LCB content in PP.

Table 13. Surface characteristics of the tested scratch specimens.

Name	COF	Roughness (Ra) (µm)
PP	0.22 ± 0.02	0.10 ± 0.02
LCBPP-5	0.24 ± 0.03	0.07 ± 0.01
LCBPP-13	0.21 ± 0.02	0.10 ± 0.01
LCBPP-19	0.20 ± 0.01	0.14 ± 0.05

5.3.6 Scratch Behavior

In a ductile polymeric system like PP, as a linearly increasing load is applied during the scratch test, a scratch groove will first form, followed by a fish-scale pattern as the damage becomes more severe. With a further increase in applied normal load, material removal by the scratch tip will ultimately occur on the scratch path [140, 148]. The onset of groove formation is the point at which the material becomes permanently deformed,

and it can be located using VLSCM height profile difference between the virgin background surface and the scratched path. The fish-scale pattern is formed due to the drawing and subsequent compressive dragging of materials by the imposing scratch tip along the scratch path [140]. The critical loads for groove formation and the onset of fish-scale are shown in Figure 28. The critical loads for the onset groove formation for the linear and LCBPPs are all close to 4.4 N. The tensile and compressive behaviors of polymers have been found to be closely associated with scratch performance. The previous numerical studies have shown that, during the scratch testing with an increasing normal load, the material experiences a complex stress state comprised of both tensile and compressive dominant triaxial stress states [140]. The parts of material beneath and behind the scratch tip experience a compressive dominant stress state and a tensile dominant stress state, respectively, and the onset of groove formation is closely related to the compressive yield stress and COF [142, 164]. Since the LCB-induced entanglement effect will only become significant upon large-scale deformation, the compressive yield stresses among the model PP systems are expected to be similar to each other. Consequently, the onset loads for the groove formation among the model PP systems are anticipated to be the same.

Figure 29 shows the optical images at the onset of fish-scale at a scratch speed of 10 mm/s. PP with 5 mol % of LCB content shows a 25% higher onset load than neat PP against the fish-scale formation. However, a further increase in LCB content has a diminishing effect on the improvement, and the scratch resistance of PP is improved by up to around 30%. This suggests that a small amount of LCB in PP is sufficient to form an effective entanglement network to enhance PP viscoelastic recovery and tensile

strength. Polymers with higher molecular weights have usually been found to be more scratch-resistant because of its higher entanglement density and higher tensile strength [146, 148]. Similarly, the LCB in PP not only increases the entanglement density of PP but also forms a stronger physical network to resist chain slippage, which increases tensile strength. The higher chain entanglement in LCBPPs is revealed through its rheological behavior [150] and the creep-recovery phenomenon shown in Figure 25. However, their tensile strength and scratch performance begin to level off after a sufficient amount of LCB (13 mol %) is incorporated.
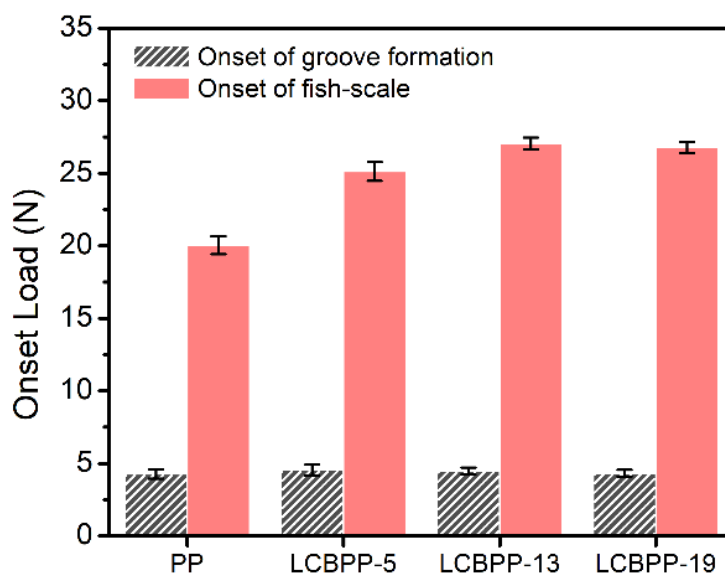
Figure 28. The critical loads for the onset of groove formation and the onset of fish-scale formation in the model systems with increasing LCB amount at 10 mm/s speed scratch test.
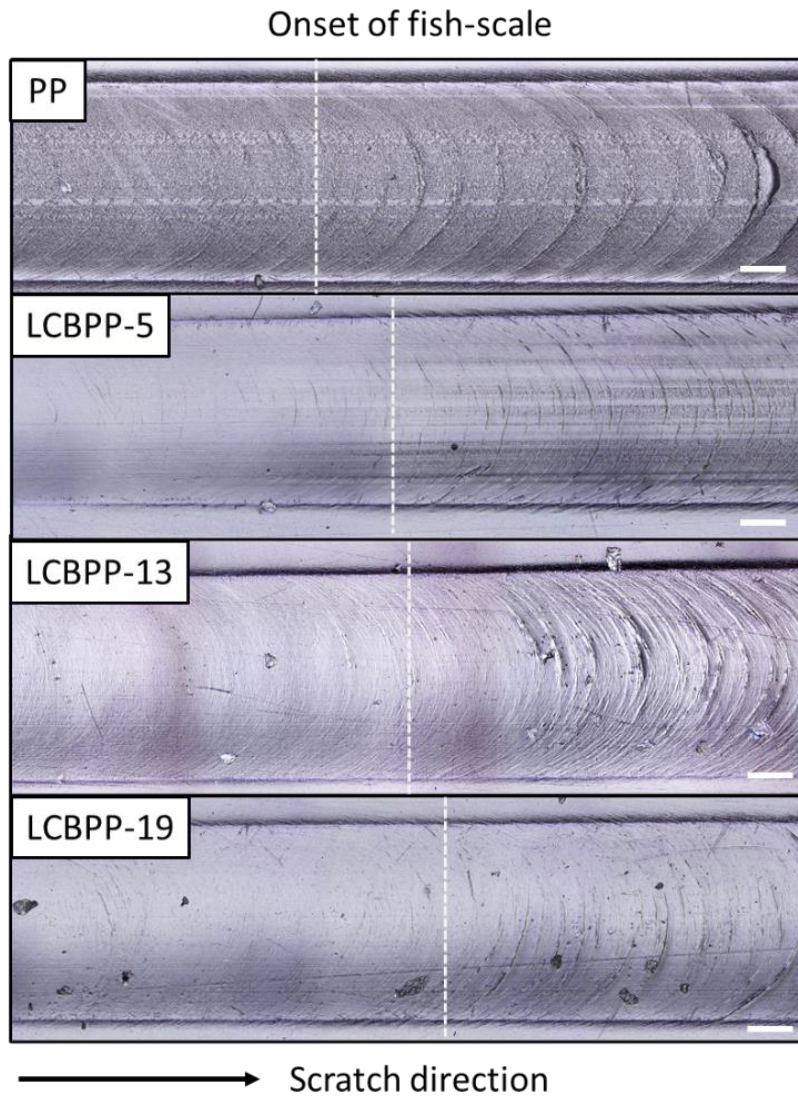
Onset of fish-scale

Figure 29. VLSCM of onset of fish-scale formation in the model linear and LCBPP
systems at 10 mm/s scratch speed. The scale bar is 100 μm.

The SCOF, defined as the ratio of tangential load to normal load at each scratching

load, is shown in Figure 30. The higher SCOF values at the higher load region in neat PP

indicate that a deeper scratch depth and damage would occur during scratching. Indeed,

as shown in Figure 31 (a), the scratch depth of linear PP departs from the LCBPPs at the

92

applied load of 15 N and becomes significantly deeper at 30 N. Increasing LCB molar fraction in PP has a negligible benefit on the scratch depth, which is consistent with the results from the microscopic analyses and the tensile properties. A residual scratch depth profile at a higher scratching speed of 100 mm/s is shown in Figure 31 (b). LCBPP-13 and LCBPP-19 exhibit much shallower scratch depths after the onset of fish-scale (25N) than those of LPP and LCBPP-5. LCBPP-5 exhibits the same residual scratch depth as LPP, suggesting that a higher scratch speed suppresses the effectiveness of LCB on the improvement of PP scratch performance.
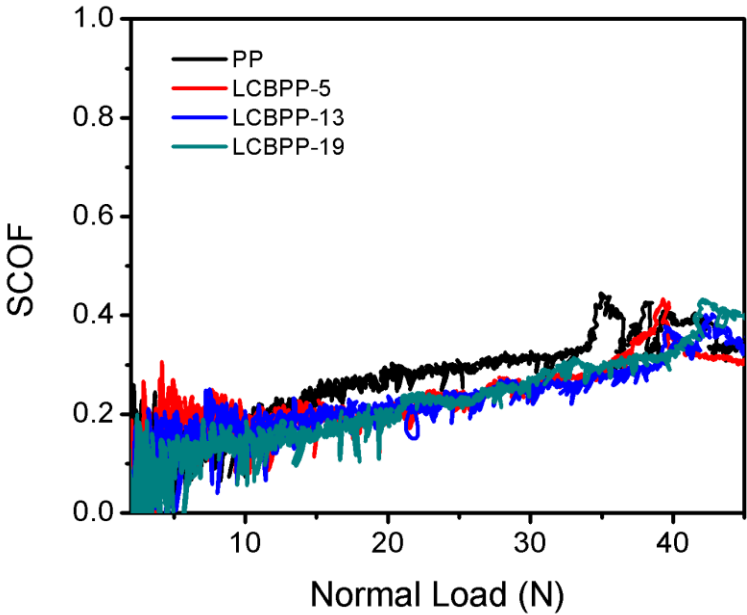
Figure 30. SCOF comparison for the model linear and LCBPPs under 10 mm/s scratch speed.
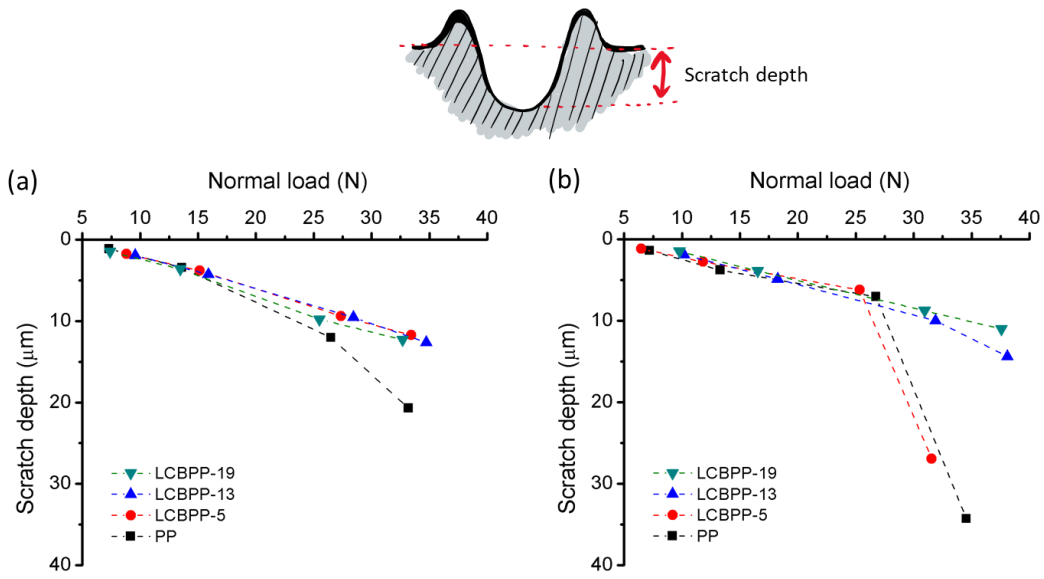
Figure 31. Scratch depth analysis at (a) 10 mm/s and (b) 100 mm/s in PP with an increasing LCB molar fraction.
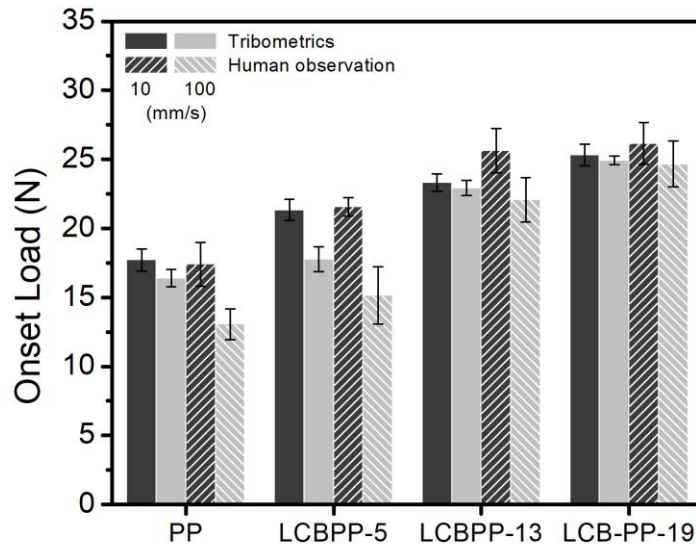
Figure 32. Onset of visibility examined by the Tribometrics software package and human assessment.

The viscoelastic nature of PP can also be observed in the scratch resistance dependency on the scratch speeds between 10 and 100 mm/s, as illustrated in Figures 32-35. The scratch resistance to deformation and damage transition was reduced at a higher testing speed of 100 mm/s. The decrease of scratch performance with increasing scratch speed is due to less time for the molecules to respond to the applied deformation, making the material more vulnerable to brittle failure and more surface damage. Browning obtained a similar trend in their scratch investigation of SAN systems [149]. While the overall scratch performance worsens with an increasing scratch speed, the improvement of the onset loads on fish-scale formation with LCB incorporation at 100 mm/s scratch speed is still up to 35%, similar to the improvement at 10 mm/s (Figure 34). However, the LCB effects on scratch performance become less noticeable in LCBPP-5. This indicates that a higher LCB molar fraction in PP might be required to effectively improve scratch performance at a higher scratching speed, which suggests that the molecular mechanisms responsible for the improved scratch performance is rate-dependent, and a high LCB molar fraction is needed to achieve sufficient cooperative molecular scale motions for enhanced properties.
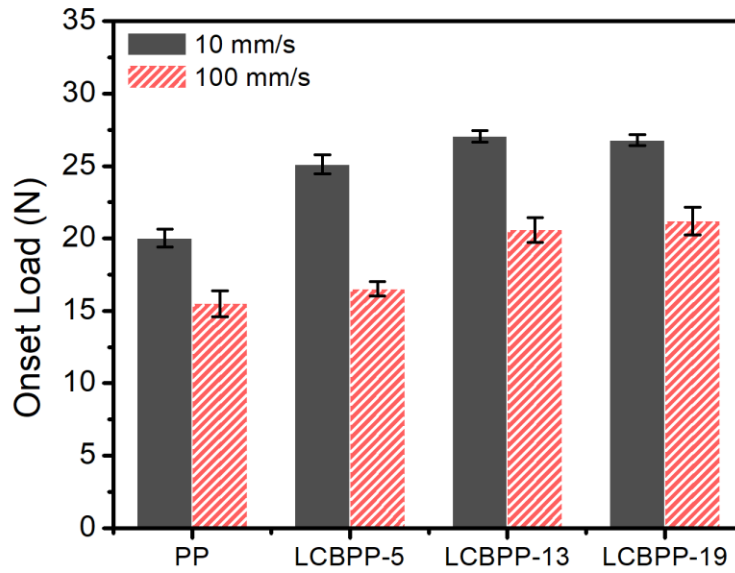
Figure 33. The onset of fish-scale at scratch speed 10 and 100 mm/s.
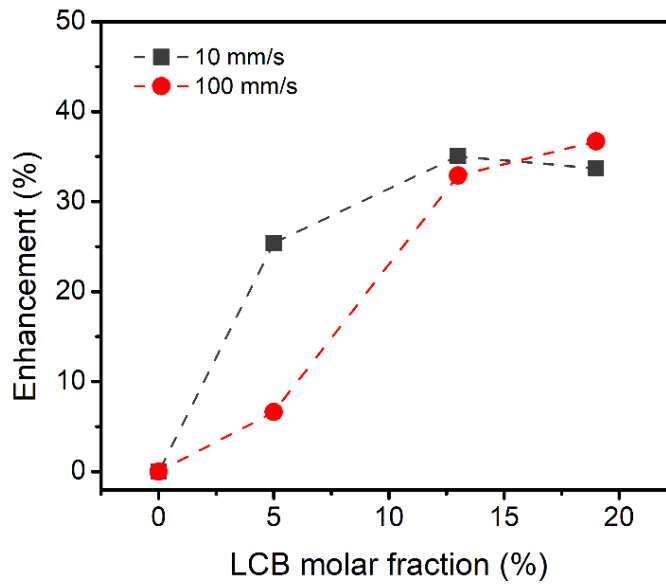
Figure 34. Enhancement percentage of the critical load of fish-scale formation with increasing LCB molar fraction.

The present study demonstrates how the LCB molar fraction influences the scratch behavior of PP. Higher tensile strength and a better elastic recovery exhibited in LCBPPs help contribute to the improved scratch performance. The present work demonstrates that LCB in the polymer matrix can be an effective way to improve scratch resistance without a need to introduce slip agents or other additives, which might cause adverse effects to the matrix. Finally, it should be noted that the present study did investigate the effect of the structural characteristics of LCB in PP on scratch behavior. It would be of interest in our future study to investigate how the branching length and number of branches influence the scratch behavior and their viscoelastic recovery, which may lead to self-healing upon scratch damage.

5.4 Conclusion

The scratch behavior of polypropylene with an increasing amount of LCB is investigated. The surface characteristics, including the COF, surface crystalline types, surface crystallinity, roughness, and crystallinities, are nearly identical among the model systems. With LCB incorporation, the scratch resistance is improved by over 30%. Further additions of LCB amounts show a minor improvement in the scratch resistance of PP. The improvement of scratch performance is attributed to the better elastic recovery and higher tensile strength of LCBPP. Incorporation 5 mol % of LCB into PP can significantly increase the entanglement density for greatly improved tensile strength and scratch performance.

CHAPTER VI

CONCLUSIONS AND FUTURE DIRECTIONS

6.1. Summary

A fundamental understanding of the relation between molecular architecture and bulk properties is of importance to designing a desirable polymeric material for commercial products and is of significant interest to the polymer science community. The challenges to achieving this goal primarily result from the inadequate methodologies to fully characterize the molecular architecture, especially for branching and crosslinking structures prepared in a post-reactor process. It is hoped this dissertation can provide fundamental knowledge of the structure-flow property relationship of high melt strength polymers. The focuses of this research effort were as follows:

- Develop the methodology to determine the molar fraction of LCB in PP quantitatively.

- Investigate the morphology of gelled particles prepared in a grafting-crosslinking post-reactor process and their effects on linear oscillatory shear properties as well as extensional flow characteristic

- Explore the effect of LCB amount on scratch resistance of PP.

- Establish the structure-flow property of polypropylene modified in a post-reactor process.

In Chapter III, the development of a new methodology to determine LCB molar fraction in PP was presented. The model PPs with a proportional amount of LCB were prepared with a specially designed coupling agent. This coupling agent is composed of an

azide group, a vinyl group, and a polymeric segment connecting these reactive groups. GPC results suggest that branching architecture are loosely branched, and branching number is ranged from 0.4 to 3.1 branch(es) per backbone. A methodology that combined the GPC and rheology with the assistance of Ngai's coupling model to determine the molar fraction of LCB in PP is proposed. The proposed method is found to be valid in another commercial LCB-containing PP as well, suggesting the great potential to apply this method to other systems.

For the project in Chapter VI, the role of the gelled particle as a soft filler to alter the rheological behavior of PP is discussed. The morphology and the content of gelled particles were first evaluated. The morphology of gelled particles from the SEM image and rheological characteristics indicates the gelled particle exhibit a core structure with dangling chains grafted on the surface. The dangling chain and chain loops on the surface of the gelled particle strongly impede the mobility of the surrounding matrix chain, contributing to higher resistance to the flow and higher elasticity of PP containing the gelled particles. The percolation threshold with consideration of core-shell structure successfully predicted the viscosity enhancement. In addition, the extensional flow viscosity suggests that incorporation of soft gelled particles can increase the entanglement density, resistance to extensional flow process, and consequently strain-hardening degree.

In Chapter V, the effect of LCB incorporation amount on scratch behavior of PP was investigated. The underlying mechanisms responsible for the enhancement in scratch resistance were explored with uniaxial tensile tests and creep-recovery measurements. LCB incorporation delays the onset of fish-scale and scratch visibility and reduces the

scratch depth along the scratch path of PP. It is found that only 5 mol% of LCB content can improve PP's scratch resistance by 25%. Further increasing LCB amount can increase scratch resistance up to 30% with 20 mol% LCB in PP. The enhancement in PP's scratch resistance is due to the better tensile property and higher elastic recovery resulting from higher entanglement density.

The present research effort provides a fundamental understanding of the structure-flow-property relationship of high melt strength PP and offers critical insights into the design of scratch-resistant PP materials with better processibility by modifying the molecular architecture, including LCB crosslinking.

6.2 Considerations for Future Work

The role of LCB and gelled particle incorporation on rheological properties of high melt strength PPs have comprehensively been studied in this dissertation. In addition, how LCB incorporation influences the scratch research and corresponded mechanism have been extensively investigated. The present study lay a vital foundation regarding methodology development in determining loosely branched LCB content in PP and providing insight regarding how to engineer material processibility and bulk properties via manipulating molecular architecture, i.e., linear to branched/crosslinked. More research efforts are still needed to explore further the effect of other branching architectures on bulk properties and gain a more comprehensive picture of the impact of molecular architecture on macroscopic response in rheology and mechanical behaviors. Some suggestions for future study are presented as follows.

6.2.1 Effect of Densely Branched Polymers on Linear Viscoelasticity

The LCB architecture discussed in this dissertation is mainly loosely grafted branching structure, i.e., 0.4-3.1 branch(es) per backbone. Research has shown that densely grafted branching polymer has distinguished differences in rheological behaviors compared to loosely grafted one. It will be of our particular interest to investigate the bottle brush, which has multiple relatively short branches distributed on the main backbone and explore its rheological behaviors. For some densely branched polymers, reduced viscosity has been found because of compact molecular structure with no entanglement; the resistance to the flow is significantly decreased [16]. The methodology proposed in the present study might be extended to this type of branching structure because of separate considerations of viscosities of linear and branched components. The mixing rule might need to be justified since there might be volume changes during the mixing of linear and highly branched polymers. To obtain the new mixing rule for these blends, the activation energy for each component can be estimated through a simple rheological measurement and the revised mixing rule.

6.2.2 Crystallization Mechanism of LCB-PPs

Branching architecture, branching degree, and branching content have been known factors influencing the crystallinity, rate of crystallization, and crystalline morphology. In the present study, the surface crystallinity remains constant after the samples are annealed, and the crystalline type of PP does not change. It is of significance to understand the effect of the amount of loosely LCB on crystalline morphology and crystalline rate for further

product mechanical properties engineering. Several studies have looked into the branching effect on the crystallization behavior of polymers; however, the results from the different groups are somewhat contrary to each other [106, 136, 158]. For example, some studies claim that branching points serve as nucleation sites to promote the crystalline formation, increase crystallinity, and reduce crystalline sizes [158]. The other group of studies believed that branching structure introduced the irregularity of molecular structure and higher resistance to chain to move in a molten state, causing less chance to form crystalline structure than the linear counterpart [136]. The inconsistency of conclusion might arise from the ill understanding of their branching structure and branching degree in LCB-containing polymer prepared by post-reactor processing. The present LCB-PP systems with well-controlled loosely grafted LCB structure can serve as a model system to investigate how the loosely grafted LCB influence the crystallization mechanism in an ambiguous way.

REFERENCES

[1] Y. Tang, C. Tzoganakis, A.E. Hamielec, J. Vlachopoulos, Peroxide crosslinking of LLDPE during reactive extrusion, Advances in Polymer Technology 9(3) (1989) 217-226.

[2] P.M. Wood-Adams, J.M. Dealy, A.W. deGroot, O.D. Redwine, Effect of molecular structure on the linear viscoelastic behavior of polyethylene, Macromolecules 33(20) (2000) 7489-7499.

[3] M. Yamaguchi, Rheological properties of linear and crosslinked polymer blends: Relation between crosslink density and enhancement of elongational viscosity, Journal of Polymer Science Part B: Polymer Physics 39(2) (2001) 228-235.

[4] W.G. Zheng, Y.H. Lee, C.B. Park, Use of nanoparticles for improving the foaming behaviors of linear PP, Journal of Applied Polymer Science 117(5) (2010) 2972-2979.

[5] T.C.B. McLeish, Tube theory of entangled polymer dynamics, Advances in Physics 51(6) (2002) 1379-1527.

[6] H. Watanabe, Viscoelasticity and dynamics of entangled polymers, Progress in Polymer Science 24(9) (1999) 1253-1403.

[7] B.E. Obi, 3 - Characterization of polymeric solids, in: B.E. Obi (Ed.), Polymeric foams structure-property-performance, William Andrew Publishing, Oxford, 2018, pp. 41-82.

[8] S.J. Dalsin, M.A. Hillmyer, F.S. Bates, Linear rheology of polyolefin-based bottlebrush polymers, Macromolecules 48(13) (2015) 4680-4691.

[9] Y.C. Lin, J. Zheng, K. Yao, H.Y. Tan, G.C. Zhang, J. Gong, T. Tang, D.H. Xu, Synthesis and linear rheological property of comb-like styrene-based polymers with a high degree of branch chain, Polymer 59 (2015) 252-259.

[10] R.M. England, S. Rimmer, Hyper/highly-branched polymers by radical polymerisations, Polymer Chemistry 1(10) (2010) 1533-1544.

[11] M. Kempf, D. Ahirwal, M. Cziep, M. Wilhelm, Synthesis and linear and nonlinear melt rheology of well-defined comb architectures of PS and PpMS with a low and controlled degree of long-chain branching, Macromolecules 46(12) (2013) 4978-4994.

[12] B. Klemm, F. Picchioni, F. van Mastrigt, P. Raffa, Starlike branched polyacrylamides by RAFT polymerization—Part I: synthesis and characterization, ACS Omega 3(12) (2018) 18762-18770.

[13] F.H. Su, H.X. Huang, Rheology and melt strength of long chain branching polypropylene prepared by reactive extrusion with various peroxides, Polymer Engineering & Science 50(2) (2010) 342-351.

[14] J.H. Tian, W. Yu, C.X. Zhou, The preparation and rheology characterization of long chain branching polypropylene, Polymer 47(23) (2006) 7962-7969.

[15] D. Auhl, J. Stange, H. Munstedt, B. Krause, D. Voigt, A. Lederer, U. Lappan, K. Lunkwitz, Long-chain branched polypropylenes by electron beam irradiation and their rheological properties, Macromolecules 37(25) (2004) 9465-9472.

[16] D. Auhl, F.J. Stadler, H. Muenstedt, Comparison of molecular structure and rheological properties of electron-beam- and gamma-irradiated polypropylene, Macromolecules 45(4) (2012) 2057-2065.

[17] X.H. Han, Y.G. Hu, M. Tang, H.G. Fang, Q.H. Wu, Z.G. Wang, Preparation and characterization of long chain branched polycarbonates with significantly enhanced environmental stress cracking behavior through gamma radiation with addition of difunctional monomer, Polymer Chemistry 7(21) (2016) 3551-3561.

[18] P.C. Hiemenz, T.P. Lodge, Polymer chemistry, Second Edition, Taylor & Francis2007.

[19] J.H. Zhao, P.S. Yu, S.H. Dong, The influence of crosslink density on the failure behavior in amorphous polymers by molecular dynamics simulations, Materials 9(4) (2016).

[20] D.H. Han, S.H. Shin, S. Petrov, Crosslinking and degradation of polypropylene by electron beam irradiation in the presence of trifunctional monomers, Radiation Physics and Chemistry 69(3) (2004) 239-244.

[21] S. Suyama, H. Ishigaki, Y. Watanabe, T. Nakamura, Crosslinking of polyethylene by dicumyl peroxide in the presence of 2,4-diphenyl-4-methyl-1-pentene, Polymer Journal 27(4) (1995) 371-375.

[22] M. Yamaguchi, Rheological properties of linear and crosslinked polymer blends: Relation between crosslink density and enhancement of elongational viscosity, Journal of Polymer Science Part B: Polymer Physics 39(2) (2001) 228-235.

[23] S.E. Zakiyan, H. Azizi, I. Ghasemi, Influence of chain mobility on rheological, dielectric and electromagnetic interference shielding properties of poly methyl-methacrylate composites filled with graphene and carbon nanotube, Composites Science and Technology 142 (2017) 10-19.

[24] M. Pollard, K. Klimke, R. Graf, H.W. Spiess, M. Wilhelm, O. Sperber, C. Piel, W. Kaminsky, Observation of chain branching in polyethylene in the solid state and melt via 13C NMR spectroscopy and melt NMR relaxation time measurements, Macromolecules 37(3) (2004) 813-825.

[25] J.C. Randall, F.J. Zoepfl, J. Silverman, A C-13 NMR-study of radiation-induced long-chain branching in polyethylene, Macromolecular Rapid Communications 4(3) (1983) 149-157.

[26] Z. Zhou, C. Anklin, R. Kuemmerle, R. Cong, X. Qiu, J. DeCesare, M.-B. Kapur, R. Patel, Very Sensitive 13C NMR method for the detection and quantification of long-chain branches in ethylene–hexene linear low-density polyethylene, Macromolecules 54(13) (2021) 5985-5990.

[27] Z. Zhou, D. Baugh, P.P. Fontaine, Y.Y. He, Z. Shi, S. Mukhopadhyay, R.J. Cong, B. Winniford, M. Miller, Long-chain branch measurement in substantially linear ethylene polymers by C-13 NMR with halogenated naphthalenes as solvents, Macromolecules 50(20) (2017) 7959-7966.

[28] Y. Ishii, M. Kida, T. Gogota, Y. Maru, K. Miyauchi, Determination of low degrees of long-chain branching in polybutadiene by double-bond hydrogenation followed by 13C NMR and DEPT spectroscopies, Polymer 185 (2019) 121965.

[29] R.N. Shroff, H. Mavridis, Assessment of NMR and rheology for the characterization of LCB in essentially linear polyethylenes, Macromolecules 34(21) (2001) 7362-7367.

[30] I. Suárez, B. Coto, Determination of long chain branching in PE samples by GPC-MALS and GPC-VIS: Comparison and uncertainties, European Polymer Journal 49(2) (2013) 492-498.

[31] W.-J. Wang, S. Kharchenko, K. Migler, S. Zhu, Triple-detector GPC characterization and processing behavior of long-chain-branched polyethylene prepared by solution polymerization with constrained geometry catalyst, Polymer 45(19) (2004) 6495-6505.

[32] L. Wild, R. Guliana, Gel permeation chromatography of polyethylene: Effect of long-chain branching, Journal of Polymer Science Part A-2: Polymer Physics 5(6) (1967) 1087-1101.

[33] B. Krause, D. Voigt, A. Lederer, D. Auhl, H. Munstedt, Determination of low amounts of long-chain branches in polypropylene using a combination of chromatographic and rheological methods, Journal of Chromatography A 1056(1-2) (2004) 217-222.

[34] J.D. Ferry, Viscoelastic properties of dilute polymer-solutions, Pure and Applied Chemistry 50(4) (1978) 299-308.

[35] J.H. Tian, W. Yu, C.X. Zhou, The preparation and rheology characterization of long chain branching polypropylene (vol 47, pg 7962, 2006), Polymer 48(7) (2007) 2186-2186.

[36] U. Kessner, J. Kaschta, F.J. Stadler, C.S. Le Duff, X. Drooghaag, H. Munstedt, Thermorheological behavior of various short- and long-chain branched polyethylenes and their correlations with the molecular structure, Macromolecules 43(17) (2010) 7341-7350.

[37] F.J. Stadler, J. Kaschta, H. Munstedt, Thermorheological behavior of various long-chain branched polyethylenes, Macromolecules 41(4) (2008) 1328-1333.

[38] Z.J. Zhang, D. Wan, H.P. Xing, Z.J. Zhang, H.Y. Tan, L. Wang, J. Zheng, Y.J. An, T. Tang, A new grafting monomer for synthesizing long chain branched polypropylene through melt radical reaction, Polymer 53(1) (2012) 121-129.

[39] Y. Amintowlieh, C. Tzoganakis, S.G. Hatzikiriakos, A. Penlidis, Effects of processing variables on polypropylene degradation and long chain branching with UV irradiation, Polymer Degradation and Stability 104 (2014) 1-10.

[40] K. Li, H.S. Zhou, Y.W. Qin, Y. Zhao, D.J. Wang, J.Y. Dong, omega-Alkenylmethyldichlorosilane-assisted propylene polymerization with Ziegler-Natta catalyst to long chain-branched polypropylene, Polymer 202 (2020).

[41] K. Li, Y.W. Qin, Y. Zhao, D.J. Wang, J.Y. Dong, Industrial adaptability of the Ziegler-Natta catalyst-friendly synthesis of long-chain-branched polypropylene based on omega-alkenylmethyldichlorosilane-assisted propylene polymerization, Industrial & Engineering Chemistry Research 60(12) (2021) 4589-4601.

[42] Y. Li, Z. Yao, S.L. Qiu, C.C. Zeng, K. Cao, Influence of molecular structure on the rheological properties and foamability of long chain branched polypropylene by "one-pot" reactive extrusion, Journal of Cellular Plastics 57(4) (2021) 433-449.

[43] Z.B. Ye, S.P. Zhu, Synthesis of branched polypropylene with isotactic backbone and atactic side chains by binary iron and zirconium single-site catalysts, Journal of Polymer Science Part A Polymer Chemistry 41(8) (2003) 1152-1159.

[44] J.A. Langston, R.H. Colby, T.C.M. Chung, F. Shimizu, T. Suzuki, M. Aoki, Synthesis and characterization of long chain branched isotactic polypropylene via metallocene catalyst and T-reagent, Macromolecules 40(8) (2007) 2712-2720.

[45] K. Li, H. Zhou, Y. Qin, Y. Zhao, D. Wang, J.-Y. Dong, ω-Alkenylmethyldichlorosilane-assisted propylene polymerization with Ziegler-Natta catalyst to long chain-branched polypropylene, Polymer 202 (2020) 122737.

[46] Y. Amintowlieh, C. Tzoganakis, A. Penlidis, Preparation and characterization of long chain branched polypropylene through UV irradiation and coagent use, Polymer-plastics Technology and Engineering 54(14) (2015) 1425-1438.

[47] T. Yang, Y. Qin, J.-Y. Dong, Nonconjugated α,ω-diolefin/propylene copolymerization to long chain-branched polypropylene by Ziegler–Natta catalyst: overcoming steric hindrance by introducing an extra electronic pulling effect, Macromolecules 51(22) (2018) 9234-9249.

[48] G.J. Song, S.J. Yang, C. Yang, X.L. She, Foaming polypropylene prepared by a novel one-step silane-grafting and crosslinking method, Journal of Porous Materials 13(3-4) (2006) 297-301.

[49] H. Liu, C.Z. Chuai, M. Iqbal, H.S. Wang, B.B. Kalsoom, M. Khattak, M.Q. Khattak, improving foam ability of polypropylene by crosslinking, Journal of Applied Polymer Science 122(2) (2011) 973-980.

[50] C.G. Yang, M.H. Wang, M.X. Zhang, X.H. Li, H.L. Wang, Z. Xing, L.F. Ye, G.Z. Wu, Supercritical CO_2 foaming of radiation cross-linked isotactic polypropylene in the presence of TAIC, Molecules 21(12) (2016).

[51] S.H. Lee, S.Y. Kim, J.R. Youn, Rheological behavior and theoretical modeling of uniaxial elongational flow properties of polypropylene/layered silicate nanocomposites, Polymer Composites 30(10) (2009) 1426-1436.

[52] M. Nofar, K. Majithiya, T. Kuboki, C.B. Park, The foamability of low-melt-strength linear polypropylene with nanoclay and coupling agent, Journal of Cellular Plastics 48(3) (2012) 271-287.

[53] Y.C. Peng, S.A. Gallegos, D.J. Gardner, Y. Han, Z.Y. Cai, Maleic anhydride polypropylene modified cellulose nanofibril polypropylene nanocomposites with enhanced impact strength, Polymer Composites 37(3) (2016) 782-793.

[54] H.B. Lu, S. Nutt, Restricted relaxation in polymer nanocomposites near the glass transition, Macromolecules 36(11) (2003) 4010-4016.

[55] K. Klimke, M. Parkinson, C. Piel, W. Kaminsky, H.W. Spiess, M. Wilhelm, Optimisation and application of polyolefin branch quantification by melt-state C-13 NMR spectroscopy, Macromolecular Chemistry and Physics 207(4) (2006) 382-395.

[56] W.Q. Weng, W.G. Hu, A.H. Dekmezian, C.J. Ruff, Long chain branched isotactic polypropylene, Macromolecules 35(10) (2002) 3838-3843.

[57] D. Yan, W.J. Wang, S. Zhu, Effect of long chain branching on rheological properties of metallocene polyethylene, Polymer 40(7) (1999) 1737-1744.

[58] Y.L. Yu, P.J. DesLauriers, D.C. Rohlfing, SEC-MALS method for the determination of long-chain branching and long-chain branching distribution in polyethylene, Polymer 46(14) (2005) 5165-5182.

[59] T. Pathaweeisariyakul, K. Narkchamnan, B. Thitisuk, W. Yau, Methods of long chain branching detection in PE by triple-detector gel permeation chromatography, Journal of Applied Polymer Science 132(28) (2015).

[60] R.N. Shroff, H. Mavridis, Long-chain-branching index for essentially linear polyethylenes, Macromolecules 32(25) (1999) 8454-8464.

[61] A.D. Gotsis, B.L.F. Zeevenhoven, C.J. Tsenoglou, Effect of long branches on the rheology of polypropylene, Journal of Rheology 48(4) (2004) 895-914.

[62] D.J. Lohse, S.T. Milner, L.J. Fetters, M. Xenidou, N. Hadjichristidis, R.A. Mendelson, C.A. Garcia-Franco, M.K. Lyon, Well-defined, model long chain branched polyethylene. 2. Melt rheological behavior, Macromolecules 35(8) (2002) 3066-3075.

[63] S.H. Tabatabaei, P.J. Carreau, A. Ajji, Rheological and thermal properties of blends of a long-chain branched polypropylene and different linear polypropylenes, Chemical Engineering Science 64(22) (2009) 4719-4731.

[64] M. Golriz, H.A. Khonakdar, J. Morshedian, Thermorheological behavior of peroxide-induced long chain branches linear low density polyethylene, Thermochimica Acta 590 (2014) 259-265.

[65] C.J. Tsenoglou, A.D. Gotsis, Rheological characterization of long chain branching in a melt of evolving molecular architecture, Macromolecules 34(14) (2001) 4685-4687.

[66] J.K. Jackson, M.E. Derosa, H.H. Winter, Molecular-Weight Dependence of relaxation-time spectra for the entanglement and flow behavior of monodisperse linear flexible polymers, Macromolecules 27(9) (1994) 2426-2431.

[67] K.L. Ngai, R.W. Rendell, A.K. Rajagopal, S. Teitler, Three coupled relations for relaxations in complex systemsa, Annals of the New York Academy of Sciences 484(1) (1986) 150-184.

[68] K.L. Ngai, R.W. Rendell, D.J. Plazek, General applicability of the coupling model to viscoelasticity of polymers: From local segmental motion to terminal flow, Journal de Physique IV 6(C8) (1996) 555-566.

[69] K.L. Ngai, A.F. Yee, Some Connections between viscoelastic properties of PVC and plasticized PVC and Molecular Kinetics, Journal of Polymer Science Part B: Polymer Physics 29(12) (1991) 1493-1501.

[70] K.L. Ngai, C.M. Roland, Terminal relaxation and diffusion of entangled three-arm star polymers: temperature and molecular weight dependencies, Journal of Polymer Science Part B: Polymer Physics 35(15) (1997) 2503-2510.

[71] J.A. Fernandes, Long-chain branched polymers and production processes, in: U.S. Patent (Ed.) United States Patent, BRASKEM AMERICA, INC. (Philadelphia, PA, US), United States, 2018.

[72] M. Yamaguchi, K.-I. Suzuki, Rheological properties and foam processability for blends of linear and crosslinked polyethylenes, Journal of Polymer Science Part B: Polymer Physics 39(18) (2001) 2159-2167.

[73] B.H. Zimm, W.H. Stockmayer, The dimensions of chain molecules containing branches and rings, The Journal of Chemical Physics 17(12) (1949) 1301-1314.

[74] C.B. Gell, W.W. Graessley, V. Efstratiadis, M. Pitsikalis, N. Hadjichristidis, Viscoelasticity and self-diffusion in melts of entangled asymmetric star polymers, Journal of Polymer Science Part B: Polymer Physics 35(12) (1997) 1943-1954.

[75] S. Trinkle, C. Friedrich, Van Gurp-Palmen-plot: a way to characterize polydispersity of linear polymers, Rheologica Acta 40(4) (2001) 322-328.

[76] S. Trinkle, P. Walter, C. Friedrich, Van Gurp-Palmen plot II - classification of long chain branched polymers by their topology, Rheologica Acta 41(1-2) (2002) 103-113.

[77] P.J. Doerpinghaus, D.G. Baird, Separating the effects of sparse long-chain branching on rheology from those due to molecular weight in polyethylenes, Journal of Rheology 47(3) (2003) 717-736.

[78] R.S. Porter, J.P. Knox, J.F. Johnson, On the flow and activation energy of branched polyethylene melts, Transactions of the Society of Rheology 12(3) (1968) 409-419.

[79] J. Janzen, R.H. Colby, Diagnosing long-chain branching in polyethylenes, Journal of Molecular Structure 485 (1999) 569-584.

[80] M.J. Struglinski, W.W. Graessley, L.J. Fetters, Effects of polydispersity on the linear viscoelastic properties of entangled polymers. 3. experimental-observations on binary-mixtures of linear and star polybutadienes, Macromolecules 21(3) (1988) 783-789.

[81] J. Stange, C. Uhl, H. Munstedt, Rheological behavior of blends from a linear and a long-chain branched polypropylene, Journal of Rheology 49(5) (2005) 1059-1079.

[82] T.J. McCallum, M. Kontopoulou, C.B. Park, E.B. Muliawan, S.G. Hatzikiriakos, The rheological and physical properties of linear and branched polypropylene blends, Polymer Engineering & Science 47(7) (2007) 1133-1140.

[83] R.G. Larson, Combinatorial rheology of branched polymer melts, Macromolecules 34(13) (2001) 4556-4571.

[84] T. Hameed, I.A. Hussein, Effect of short chain branching of LDPE on its miscibility with linear HDPE, Macromolecular Materials and Engineering 289(2) (2004) 198-203.

[85] J. Stange, S. Wachter, H. Munstedt, H. Kaspar, Linear rheological properties of the semifluorinated copolymer tetrafluoroethylene-hexafluoropropylene-vinylidenfluoride (THV) with controlled amounts of long-chain branching, Macromolecules 40(7) (2007) 2409-2416.

[86] W.E. Rochefort, G.G. Smith, H. Rachapudy, V.R. Raju, W.W. Graessley, Properties of Amorphous and Crystallizable Hydrocarbon Polymers .2. rheology of Linear and Star-Branched Polybutadiene, Journal of Polymer Science Part B: Polymer Physics 17(7) (1979) 1197-1210.

[87] J.P. Busnel, F. Foucault, L. Denis, W. Lee, T. Chang, Investigation and interpretation of band broadening in size exclusion chromatography, Journal of Chromatography A 930(1-2) (2001) 61-71.

[88] S. Zhou, S.C. Zhao, Z. Xin, W.X. Wang, A Novel Strategy for Achieving High melt strength polypropylene and an investigation of its foamability, Journal of Macromolecular Science, Part B 53(10) (2014) 1695-1714.

[89] S. Doroudiani, C.B. Park, M.T. Kortschot, Processing and characterization of microcellular foamed high-density polythylene/isotactic polypropylene blends, Polymer Engineering & Science 38(7) (1998) 1205-1215.

[90] S. Bhattacharya, R.K. Gupta, M. Jollands, S.N. Bhattacharya, Foaming behavior of high-melt strength polypropylene/clay nanocomposites, Polymer Engineering & Science 49(10) (2009) 2070-2084.

[91] F. Yoshii, K. Makuuchi, S. Kikukawa, T. Tanaka, J. Saitoh, K. Koyama, High-melt-strength polypropylene with electron beam irradiation in the presence of polyfunctional monomers, Journal of Applied Polymer Science 60(4) (1996) 617-623.

[92] K.J. Kim, Y.S. Ok, B.K. Kim, Crosslinking of polyethylene with peroxide and multifunctional monomers during extrusion, European Polymer Journal 28(12) (1992) 1487-1491.

[93] F. Kamleitner, B. Duscher, T. Koch, S. Knaus, K. Schmid, V.M. Archodoulaki, Influence of the molar mass on long-chain branching of polypropylene, Polymers 9(9) (2017).

[94] X.C. Wang, C. Tzoganakis, G.L. Rempel, Chemical modification of polypropylene with peroxide/pentaerythritol triacrylate by reactive extrusion, Journal of Applied Polymer Science 61(8) (1996) 1395-1404.

[95] Y. Li, S. Jia, S. Du, Y. Wang, L. Lv, J. Zhang, Improved properties of recycled polypropylene by introducing the long chain branched structure through reactive extrusion, Waste Management 76 (2018) 172-179.

[96] Y. An, Z. Zhang, Y. Wang, J. Qiu, T. Tang, Structure and properties of high melt strength polypropylene prepared by combined method of blending and crosslinking, Journal of Applied Polymer Science 116(3) (2010) 1739-1746.

[97] T. Chen, H.J. Qian, Y.L. Zhu, Z.Y. Lu, Structure and Dynamics Properties at Interphase Region in the Composite of Polystyrene and Cross-Linked Polystyrene Soft Nanoparticle, Macromolecules 48(8) (2015) 2751-2760.

[98] T. Chen, H.Y. Zhao, R. Shi, W.F. Lin, X.M. Jia, H.J. Qian, Z.Y. Lu, X.X. Zhang, Y.K. Li, Z.Y. Sun, An unexpected N-dependence in the viscosity reduction in all-polymer nanocomposite, Nature Communications 10 (2019).

[99] U.M. Shrestha, L. Han, T. Saito, K.S. Schweizer, M.D. Dadmun, Mechanism of Soft Nanoparticle diffusion in entangled polymer melts, Macromolecules 53(17) (2020) 7580-7589.

[100] M.E. Mackay, T.T. Dao, A. Tuteja, D.L. Ho, B. Van Horn, H.C. Kim, C.J. Hawker, Nanoscale effects leading to non-Einstein-like decrease in viscosity, Nature Materials 2(11) (2003) 762-766.

[101] F.B. Wyart, P.G. de Gennes, Viscosity at small scales in polymer melts, The European Physical Journal E 1(1) (2000) 93-97.

[102] L.H. Cai, S. Panyukov, M. Rubinstein, Mobility of nonsticky nanoparticles in polymer Liquids, Macromolecules 44(19) (2011) 7853-7863.

[103] S. Rostom, M.D. Dadmun, The impact of nanoparticle softness on its tracer diffusion coefficient in all polymer nanocomposites, Journal of Applied Physics 127(7) (2020).

[104] Y.J. Hou, B.H. Xie, W. Yang, M.B. Yang, Micro-structure and fracture behavior of high-melt-strength PPs prepared by reactive extrusion, Journal of Macromolecular Science, Part B 51(1-3) (2012) 48-59.

[105] B.-R. Sheng, B.-H. Xie, W. Yang, Q.-G. Li, M.-B. Yang, Structure and properties of reactive extruded ethylene-block-co-polypropylene: influence of dicumyl peroxide and divinylbenzene, Journal of Macromolecular Science, Part B 47(6) (2008) 1236-1250.

[106] W. Zhao, Y. Huang, X. Liao, Q. Yang, The molecular structure characteristics of long chain branched polypropylene and its effects on non-isothermal crystallization and mechanical properties, Polymer 54(4) (2013) 1455-1462.

[107] A.C. Ouano, P.L. Mercier, The molecular weight distribution of polypropylene, Journal of Polymer Science Part C: Polymer Symposia 21(1) (1968) 309-315.

[108] W.J. Wang, S. Kharchenko, K. Migler, S.P. Zhu, Triple-detector GPC characterization and processing behavior of long-chain-branched polyethylene prepared by solution polymerization with constrained geometry catalyst, Polymer 45(19) (2004) 6495-6505.

[109] K.-S. Lee, Y.-W. Chang, Thermal, mechanical, and rheological properties of poly(ε-caprolactone)/halloysite nanotube nanocomposites, Journal of Applied Polymer Science 128(5) (2013) 2807-2816.

[110] M. Bek, J. Gonzalez-Gutierrez, C. Kukla, K.P. Cresnar, B. Maroh, L.S. Perse, Rheological behaviour of highly filled materials for injection moulding and additive manufacturing: effect of particle material and loading, Applied Sciences 10(22) (2020).

[111] D. Wu, L. Wu, Y. Sun, M. Zhang, Rheological properties and crystallization behavior of multi-walled carbon nanotube/poly(ε-caprolactone) composites, Journal of Polymer Science Part B: Polymer Physics 45(23) (2007) 3137-3147.

[112] T. Yokohara, S. Nobukawa, M. Yamaguchi, Rheological properties of polymer composites with flexible fine fibers, Journal of Rheology 55(6) (2011) 1205-1218.

[113] C.M. Koo, M.J. Kim, M.H. Choi, S.O. Kim, I.J. Chung, Mechanical and rheological properties of the maleated polypropylene-layered silicate nanocomposites with different morphology, Journal of Applied Polymer Science 88(6) (2003) 1526-1535.
[114] S. Karamipour, H. Ebadi-Dehaghani, D. Ashouri, S. Mousavian, Effect of nano-CaCO3 on rheological and dynamic mechanical properties of polypropylene: Experiments and models, Polymer Testing 30(1) (2011) 110-117.

[115] S. Li, G. He, X. Liao, C.B. Park, Q. Yang, G. Li, Introduction of a long-chain branching structure by ultraviolet-induced reactive extrusion to improve cell morphology and processing properties of polylactide foam, RSC Advances 7(11) (2017) 6266-6277.

[116] F. Wu, B. Zhang, W. Yang, Z. Liu, M. Yang, Inorganic silica functionalized with PLLA chains via grafting methods to enhance the melt strength of PLLA/silica nanocomposites, Polymer 55(22) (2014) 5760-5772.

[117] F.T. Trouton, On the coefficient of viscous traction and its relation to that of viscosity, Proceedings of the Royal Society of London. Series A 77(519) (1906) 426-440.

[118] A. Mujtaba, M. Keller, S. Ilisch, H.J. Radusch, M. Beiner, T. Thurn-Albrecht, K. Saalwächter, Detection of surface-immobilized components and their role in viscoelastic reinforcement of rubber–silica nanocomposites, ACS Macro Letters 3(5) (2014) 481-485.

[119] Z. Zheng, Y. Song, R. Yang, Q. Zheng, Direct evidence for percolation of immobilized polymer layer around nanoparticles accounting for sol–gel transition in fumed silica dispersions, Langmuir 31(50) (2015) 13478-13487.

[120] J. Berriot, H. Montes, F. Lequeux, D. Long, P. Sotta, Evidence for the shift of the glass transition near the particles in silica-filled elastomers, Macromolecules 35(26) (2002) 9756-9762.

[121] D. Long, P. Sotta, Stress relaxation of large amplitudes and long timescales in soft thermoplastic and filled elastomers, Rheologica Acta 46(8) (2007) 1029-1044.

[122] L.J. Fetters, D.J. Lohse, R.H. Colby, Chain Dimensions and Entanglement Spacings, in: J.E. Mark (Ed.), Physical properties of polymers handbook, Springer New York, New York, NY, 2007, pp. 447-454.

[123] K.D. Kumar, A.H. Tsou, A.K. Bhowmick, Unique tackification behavior of needle-like sepiolite nanoclay in brominated isobutylene-co-p-methylstyrene (BIMS) rubber, Macromolecules 43(9) (2010) 4184-4193.

[124] C. Liu, J. He, E.v. Ruymbeke, R. Keunings, C. Bailly, Evaluation of different methods for the determination of the plateau modulus and the entanglement molecular weight, Polymer 47(13) (2006) 4461-4479.

[125] S. Franco, E. Buratti, B. Ruzicka, V. Nigro, N. Zoratto, P. Matricardi, E. Zaccarelli, R. Angelini, Volume fraction determination of microgel composed of interpenetrating polymer networks of PNIPAM and polyacrylic acid, Journal of Physics: Condensed Matter 33(17) (2021).

[126] M.A. López Manchado, J. Biagiotti, J.M. Kenny, Rheological behavior and processability of polypropylene blends with rubber ethylene propylene diene terpolymer, Journal of Applied Polymer Science 81(1) (2001) 1-10.

[127] M.M. Cross, Rheology of non-Newtonian fluids: A new flow equation for pseudoplastic systems, Journal of Colloid Science 20(5) (1965) 417-437.

[128] E. Senses, S. Darvishi, M.S. Tyagi, A. Faraone, Entangled polymer dynamics in attractive nanocomposite melts, Macromolecules 53(12) (2020) 4982-4989.

[129] R. Mangal, S. Srivastava, L.A. Archer, Phase stability and dynamics of entangled polymer–nanoparticle composites, Nature Communications 6(1) (2015) 7198.

[130] W. You, W.Z. Cui, W. Yu, Decoupling hydrodynamic and entanglement effects on the modulus reinforcement of grafted silica filled nanocomposites through Thermal and rheological features, Polymer 213 (2021).

[131] K.L. White, H. Yao, X. Zhang, H.-J. Sue, Rheology of electrostatically tethered nanoplatelets and multi-walled carbon nanotubes in epoxy, Polymer 84 (2016) 223-233.

[132] M.P. da SiIva, S.N. Cavalcanti, A.M. Alves, D.M.G. Freitas, P. Agrawal, E.O. Vilar, T.J.A. de Mélo, Evaluation of the rheological and electrical percolation of high-density polyethylene/carbon black composites using mathematical models, Polymer Engineering & Science 61(7) (2021) 2105-2116.

[133] S. Cheng, V. Bocharova, A. Belianinov, S. Xiong, A. Kisliuk, S. Somnath, A.P. Holt, O.S. Ovchinnikova, S. Jesse, H. Martin, T. Etampawala, M. Dadmun, A.P. Sokolov, Unraveling the mechanism of nanoscale mechanical reinforcement in glassy polymer nanocomposites, Nano Letters 16(6) (2016) 3630-3637.

[134] Q. Chen, S. Gong, J. Moll, D. Zhao, S.K. Kumar, R.H. Colby, Mechanical reinforcement of polymer nanocomposites from percolation of a nanoparticle network, ACS Macro Letters 4(4) (2015) 398-402.

[135] Y.C. Li, S. Jia, S.L. Du, Y.F. Wang, L.D. Lv, J.B. Zhang, Improved properties of recycled polypropylene by introducing the long chain branched structure through reactive extrusion, Waste Management 76 (2018) 172-179.

[136] G.L. Wang, B.H. Guo, R. Li, Synthesis, characterization, and properties of long-chain branched poly(butylene succinate), Journal of Applied Polymer Science 124(2) (2012) 1271-1280.

[137] W.Y. Zhao, Y.J. Huang, X. Liao, Q. Yang, The molecular structure characteristics of long chain branched polypropylene and its effects on non-isothermal crystallization and mechanical properties, Polymer 54(4) (2013) 1455-1462.

[138] ISO 19252:2008. Plastics – Determination of scratch properties, International Organization for Standardization, 2008.

[139] ASTM. D7027-13 Standard test method for evaluation of scratch resistance of polymeric coatings and plastics using an instrumented scratch machine., ASTM International, West Conshohocken, PA, 2013.

[140] H. Jiang, R. Browning, H.J. Sue, Understanding of scratch-induced damage mechanisms in polymers, Polymer 50(16) (2009) 4056-4065.

[141] M.M. Hossain, R. Minkwitz, P. Charoensirisomboon, H.J. Sue, Quantitative modeling of scratch-induced deformation in amorphous polymers, Polymer 55(23) (2014) 6152-6166.

[142] S. Xiao, M.M. Hossain, P. Liu, H.L. Wang, F.C. Hu, H.J. Sue, Scratch behavior of model polyurethane elastomers containing different soft segment types, Materials & Design 132 (2017) 419-429.

[143] G. Molero, H.-J. Sue, Scratch behavior of model epoxy resins with different crosslinking densities, Materials & Design 182 (2019) 107965.

[144] S.R. Du, M. Mullins, M. Hamdi, H.J. Sue, Quantitative modeling of scratch behavior of amorphous polymers at elevated temperatures, Polymer 197 (2020).

[145] C.S. Schollenberger, K. Dinbergs, Thermoplastic polyurethane elastomer molecular weight-property relations - further-studies, Journal of Elastomers & Plastics 11(1) (1979) 58-91.

[146] S. Xiao, H.J. Sue, Effect of molecular weight on scratch and abrasive wear behaviors of thermoplastic polyurethane elastomers, Polymer 169 (2019) 124-130.

[147] H.W. Mccormick, F.M. Brower, L. Kin, The Effect of molecular weight distribution on the physical properties of polystyrene, Journal of Polymer Science 39(135) (1959) 87-100.

[148] E. Moghbelli, R.L. Browning, W.J. Boo, S.F. Hahn, L.J.E. Feick, H.J. Sue, Effects of molecular weight and thermal history on scratch behavior of polypropylene thin sheets, Tribology International 41(5) (2008) 425-433.

[149] R. Browning, H.J. Sue, R. Minkwitz, P. Charoensirisomboon, Effects of acrylonitrile content and molecular weight on the scratch behavior of styrene-acrylonitrile random copolymers, Polymer Engineering & Science 51(11) (2011) 2282-2294.

[150] C.-Y. Tsai, C.-S. Chang, H.-J. Sue, Quantification of long-chain branching molar fraction in polypropylene, Industrial & Engineering Chemistry Research 60(9) (2021) 3770-3778.

[151] B. Na, K. Wang, Q. Zhang, R. Du, Q. Fu, Tensile properties in the oriented blends of high-density polyethylene and isotactic polypropylene obtained by dynamic packing injection molding, Polymer 46(9) (2005) 3190-3198.

[152] A.T. Jones, J.M. Aizlewood, D.R. Beckett, Crystalline forms of isotactic polypropylene, Die Makromolekulare Chemie 75 (1964) 134-158.

[153] M. Iijima, G. Strobl, Isothermal crystallization and melting of isotactic polypropylene analyzed by time- and temperature-dependent small-angle X-ray scattering experiments, Macromolecules 33(14) (2000) 5204-5214.

[154] P. Tordjeman, C. Robert, G. Marin, P. Gerard, The effect of α, β crystalline structure on the mechanical properties of polypropylene, The European Physical Journal E 4(4) (2001) 459-465.

[155] T. Labour, C. Gauthier, R. Séguéla, G. Vigier, Y. Bomal, G. Orange, Influence of the β crystalline phase on the mechanical properties of unfilled and CaCO3-filled polypropylene. I. Structural and mechanical characterisation, Polymer 42(16) (2001) 7127-7135.

[156] P. Liu, K.L. White, H. Sugiyama, J. Xi, T. Higuchi, T. Hoshino, R. Ishige, H. Jinnai, A. Takahara, H.J. Sue, Influence of trace amount of well-dispersed carbon nanotubes on structural development and tensile properties of polypropylene, Macromolecules 46(2) (2013) 463-473.

[157] A.T. Jones, J.M. Aizlewood, D.R. Beckett, Crystalline forms of isotactic polypropylene, Die Makromolekulare Chemie 75(1) (1964) 134-158.

[158] M. Nofar, W.L. Zhu, C.B. Park, J. Randall, Crystallization kinetics of linear and long-chain-branched polylactide, Industrial & Engineering Chemistry Research 50(24) (2011) 13789-13798.

[159] R.N. Haward, The physics of glassy polymers, Applied Science Publishers, London, 1973.

[160] S. Humbert, O. Lame, R. Séguéla, G. Vigier, A re-examination of the elastic modulus dependence on crystallinity in semi-crystalline polymers, Polymer 52(21) (2011) 4899-4909.

[161] R.W. Nunes, J.R. Martin, J.F. Johnson, Influence of molecular-weight and molecular-weight distribution on mechanical-properties of polymers, Polymer Engineering & Science 22(4) (1982) 205-228.

[162] K. Balani, V. Verma, A. Agarwal, R. Narayan, Physical, Thermal, and Mechanical Properties of Polymers, Biosurfaces (2014) 329-344.

[163] C.S. Schollenberger, K. Dinbergs, Thermoplastic polyurethane elastomer molecular weight-property relations - further-studies, Journal of Elastomers & Plastics 11(1) (1979) 58-91

[164] M.M. Hossain, R. Minkwitz, H.J. Sue, Minimization of surface friction effect on scratch-induced deformation in polymers, Polymer Engineering & Science 53(7) (2013) 1405-1413.